Electronic Supporting Information File

Odd-Even Effect Controls Twist-Elasticity of an Organic Fluorophore in Cocrystals Prepared Using Mechanochemistry

Nabadeep Kalita,[a] Poonam Deka,[a] Ishita Ghosh,[b] Kalyan J. Kalita,[b] Ashish Gogoi,[a] C. Malla Reddy*[,c] and Ranjit Thakuria*[,a]

[a] Department of Chemistry, Gauhati University, Guwahati 781014, Assam, India. E-mail: ranjit.thakuria@gmail.com, ranjit.thakuria@gauhati.ac.in

[b] Department of Chemical Sciences, Indian Institute of Science Education and Research Kolkata, 741246, West Bengal, India.

[c] Department of Chemistry, Indian Institute of Technology Hyderabad, Telangana 502285, India.

Table of Content

1. Experimental Section

Materials

3-pyridineacetonitrile, biphenyl-4-carboxaldehyde and piperidine were purchased from Sigma-Aldrich and used without further purification. All the aliphatic dicarboxylic acids were purchased from local suppliers and used without further purification.

Cocrystal Synthesis:

Liquid-assisted grinding (LAG) in presence of catalytic amount of acetonitrile as liquid is used to prepare cocrystals of **PDAN-1** with aliphatic dicarboxylic acids varying chain lengths from oxalic acid (**C_2**) to sebacic acid (**C_{10}**) along with two unsaturated diacids viz. maleic acid (**MEA**) and fumaric acid (**FA**). All the co-crystallization experiments resulted in the formation of 2:1 cocrystals except with OA and MEA, which resulted in the formation of 1:1 molecular salts based on SCXRD and PXRD analysis. Details of the synthetic procedure are given below.

PDAN-1•OA salt Cocrystal

PDAN-1P (28.2 mg, 0.1 mmol) and **oxalic acid** (12.6 mg, 0.1 mmol) in 1:1 stoichiometry were ground in a mortar pestle in presence of catalytic amount (100 μL) of acetonitrile solvent for about 15 minutes. The solution crystallization of the ground material in a mixture of chloroform, acetonitrile and methanol (3:1:1) solvent afforded block shaped single crystals of the product.

PDAN-1•MA Cocrystal

PDAN-1P (56.4 mg, 0.2 mmol) and **malonic acid** (10.4 mg, 0.1 mmol) in 2:1 stoichiometry were ground in a mortar pestle in presence of catalytic amount (100 μL) of acetonitrile solvent for about 15 minutes. The solution crystallization of the ground material in a mixture of chloroform and acetonitrile (3:1) solvent afforded block shaped single crystals of the product.

PDAN-1•SA Cocrystal

PDAN-1P (56.4 mg, 0.2 mmol) and **succinic acid** (11.8 mg, 0.1 mmol) in 2:1 stoichiometry were ground in a mortar pestle in presence of catalytic amount (100 μL) of acetonitrile solvent

for about 15 minutes. The solution crystallization of the ground material in a mixture of chloroform and acetonitrile (3:1) solvent afforded block shaped single crystals of the product.

PDAN-1•GA Cocrystal

PDAN-1P (56.4 mg, 0.2 mmol) and **glutaric acid** (13.2 mg, 0.1 mmol) in 2:1 stoichiometry were ground in a mortar pestle in presence of catalytic amount (100 μL) of acetonitrile solvent for about 15 minutes. The solution crystallization of the ground material in a mixture of chloroform and acetonitrile (3:1) solvent afforded block shaped single crystals of the product.

PDAN-1•AA Cocrystal

PDAN-1P (56.4 mg, 0.2 mmol) and **adipic acid** (14.6 mg, 0.1 mmol) in 2:1 stoichiometry were ground in a mortar pestle in presence of catalytic amount (100 μL) of acetonitrile solvent for about 15 minutes.The solution crystallization of the ground material in a mixture of chloroform and acetonitrile (3:1) solvent afforded block shaped single crystals of the product.

PDAN-1•PMA Cocrystal

PDAN-1P (56.4 mg, 0.2 mmol) and **pimelic acid** (16.0 mg, 0.1 mmol) in 2:1 stoichiometry were ground in a mortar pestle in presence of catalytic amount (100 μL) of acetonitrile solvent for about 15 minutes. After several batches of solution crystallization, we were not able to generate suitable single crystals of the ground materials for structure elucidation using SCXRD.

PDAN-1•SUBE Cocrystal

PDAN-1P (56.4 mg, 0.2 mmol) and **suberic acid** (17.4 mg, 0.1 mmol) in 2:1 stoichiometry were ground in a mortar pestle in presence of catalytic amount (100 μL) of acetonitrile solvent for about 15 minutes. After several batches of solution crystallization, we were not able to generate suitable single crystals of the ground materials for structure elucidation using SCXRD.

PDAN-1•AZA Cocrystal

PDAN-1P (56.4 mg, 0.2 mmol) and **azelaic acid** (18.8 mg, 0.1 mmol) in 2:1 stoichiometry were ground in a mortar pestle in presence of catalytic amount (100 μL) of acetonitrile solvent for

about 15 minutes.The solution crystallization of the ground material in a mixture of chloroform, acetonitrile and methanol (3:1:0.5) solvent afforded block shaped single crystal of the product.

PDAN-1•SEBA Cocrystal

PDAN-1P (56.4 mg, 0.2 mmol) and **sebacic acid** (20.2 mg, 0.1 mmol) in 2:1 stoichiometry were ground in a mortar pestle in presence of catalytic amount (100 μL) of acetonitrile solvent for about 15 minutes. The solution crystallization of the ground material in a mixture of chloroform, acetonitrile and methanol (3:1:0.5) solvent afforded block shaped single crystal of the product.

PDAN-1•MEA molecular salt

PDAN-1P (28.2 mg, 0.1 mmol) and **maleic acid** (11.6 mg, 0.1 mmol) in 1:1 stoichiometry were ground in a mortar pestle in presence of catalytic amount (100 μL) of acetonitrile solvent for about 15 minutes. The solution crystallization of the ground material in a mixture of chloroform and acetonitrile (3:1) solvent afforded block shaped single crystal of the product.

PDAN-1•FA Cocrystal

PDAN-1P (56.4 mg, 0.2 mmol) and **fumaric acid** (11.6 mg, 0.1 mmol) in 2:1 stoichiometry were ground in a mortar pestle in presence of catalytic amount (100 μL) of acetonitrile solvent for about 15 minutes. The solution crystallization of the ground material in a mixture of chloroform, acetonitrile and methanol (3:1:0.5) solvent afforded block shaped single crystal of the product.

2. Instrumental Details

Powder X-ray diffraction (PXRD)

PXRD measurements were performed at room temperature on a Rigaku Ultima IV X-ray powder diffractometer operating with a Cu Kα X-ray source, equipped with a Ni filter to suppress Kβ emission and a D/teX Ultra high-speed position sensitive detector, with a scan range 2θ = 5-50°, step size of 0.02° and scan rate of 10° min^{-1}.

Single crystal X-ray diffraction

Single crystal X-ray diffraction (SCXRD) data of all the compounds were collected on a Bruker SMART APEX II CCD diffractometer equipped with a graphite monochromator and a Mo Kα fine-focus sealed tube (λ = 0.71073 Å). Data integration was done using SAINT. Intensities for absorption were corrected using SADABS. Structure solution and refinement were carried out using Bruker SHELXTL. The hydrogen atoms were refined isotropically, and all the other atoms were refined anisotropically. C−H hydrogens were fixed using the HFIX command in SHELXTL. Molecular graphics were prepared using X-SEED and Mercury licensed version 4.2.

Thermal analysis

DSC measurements were performed on a Mettler Toledo DSC instrument with a temperature range 25–400 °C and heating rate of 10 °C min^{-1} on sample on 40 μL aluminium pan with pin-hole lid under an ultra-high pure nitrogen environment purged at 40 mL min^{-1}. For the **PDAN-1B** two additional heating rates viz. 5 °C min^{-1} and 20 °C min^{-1} was used for thermal measurements.

Nanoindentation

Crystals were mounted using cyanoacrylate glue on a stainless-steel disk-shaped sample holder having a smooth surface in such an orientation so that the major faces would be indented. The experiments were carried out using a nanoindenter (Hysitron Triboindenter, TI Premier, Minneapolis, USA) with a three-sided pyramidal Berkovich diamond indenter tip of radius 150 nm having an in-situ Scanning Probe Microscopy (SPM) facility. Before nanoindentation, the tip area function was calculated from a series of indentations on a standard fused quartz sample. The indentations were performed under the load control mode fixing the maximum load constant (P_{max}) at 6 mN. The rates of loading and unloading were both 1200 μN s^{-1} with 5 sec duration and a 2 sec holding period was applied at the maximum indentation depth. SPM images of the indentation impressions were captured immediately just after unloading to avoid any time dependent elastic shape recovery of the residual impressions. The obtained *P*−*h* curves were analyzed using the standard Oliver−Pharr method to extract the required parameters, elastic modulus (*E*), and hardness (*H*) of the crystals.

Fluorescence lifetime study

The fluorescence decay profile was performed using time-correlated single-photon counting (TCSPC) methods with HORIBA JOBIN YVON (single photon counting controller: Fluorohub, precision photo multiplier power supply: Fluoro3PS). For molecular excitation 371 nm, Nano-LED was used as a light source and an MCP photomultiplier tube (PMT) (Hamamatsu R3809U-50 series) was used as the detector and the decay was collected with 50 ns TAC range. Photoluminescence (PL) decay profiles were collected in a solid state and fitted multi-exponentially as indicated, and the average lifetime was considered for discussion.

3. PXRD analysis

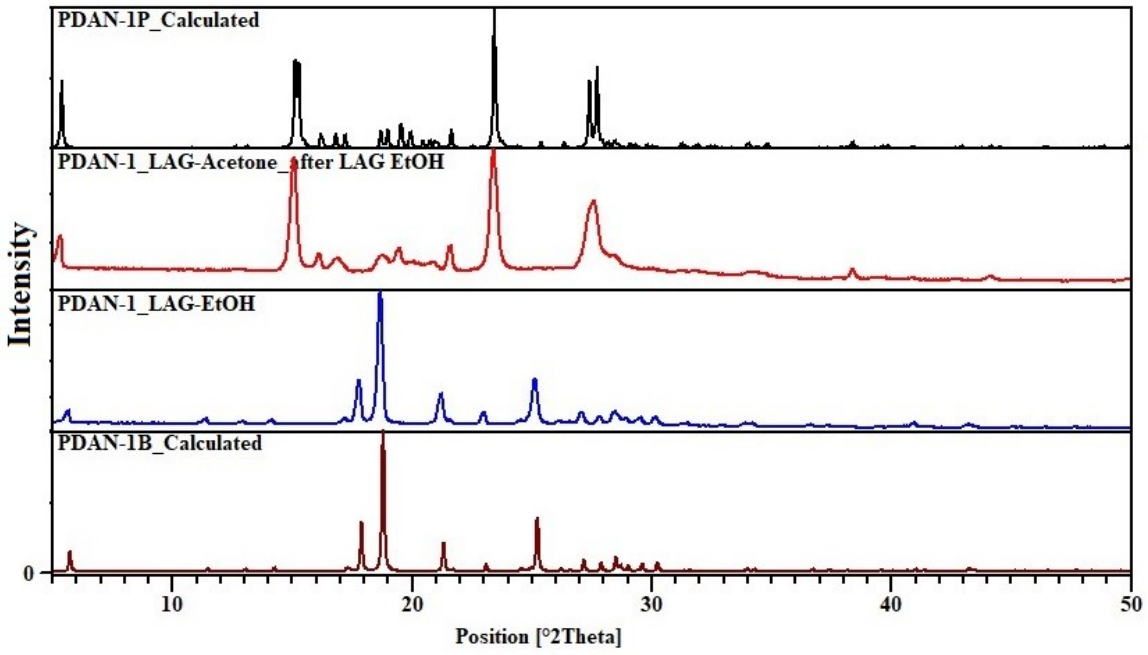

(a)

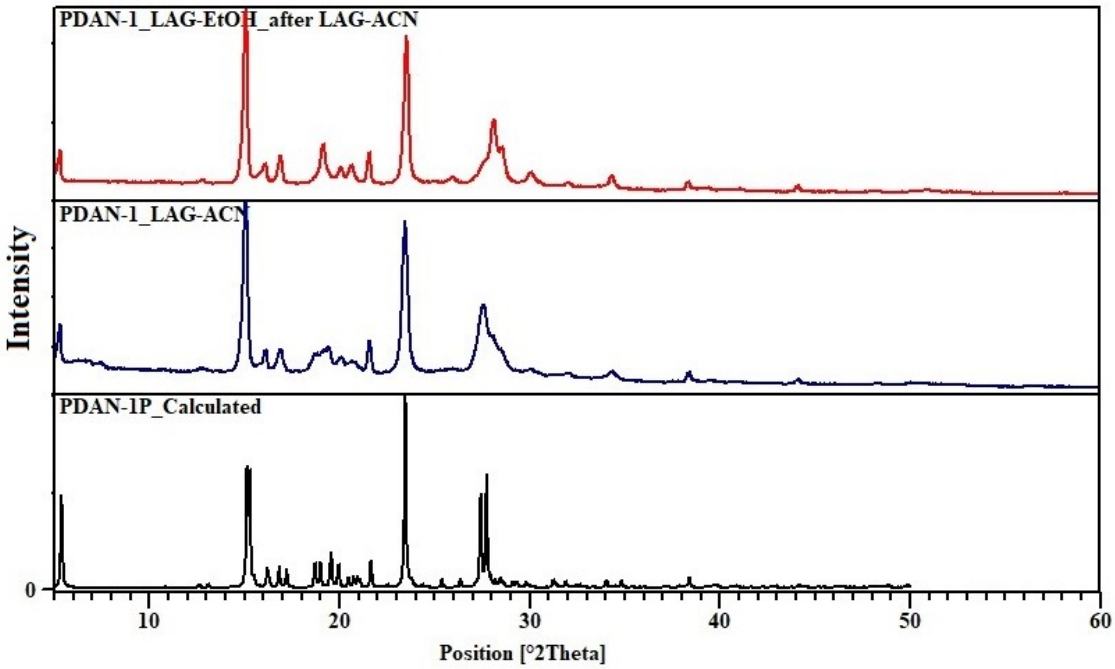

(b)

Figure S1. (a) Stack plots of PXRD patterns of the ground materials that show conversion of **PDAN-1B** to **PDAN-1P** form under mechanochemical condition; (b) stack plots of PXRD patterns of the ground materials that show irreversible nature of **PDAN-1P** form under mechanochemical condition.

4. Thermal analysis

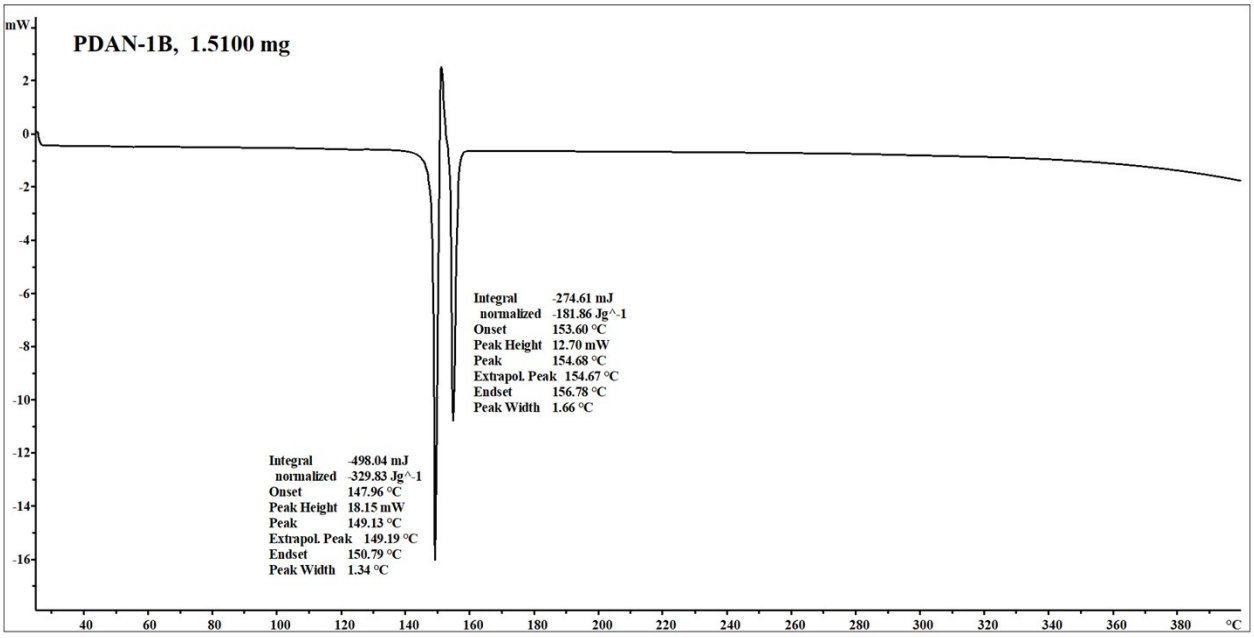

(a)

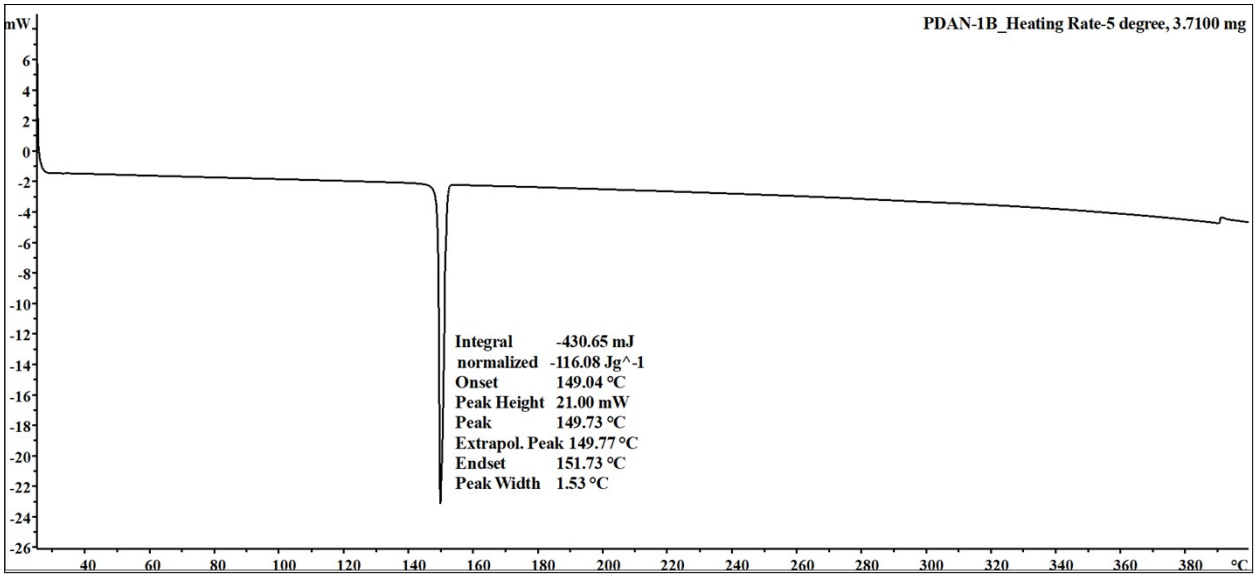
PDAN-1B_Heating Rate-5 degree, 3.7100 mg
mW
Integral -430.65 mJ
normalized -116.08 Jg^-1
Onset 149.04 °C
Peak Height 21.00 mW
Peak 149.73 °C
Extrapol. Peak 149.77 °C
Endset 151.73 °C
Peak Width 1.53 °C
°C

(b)

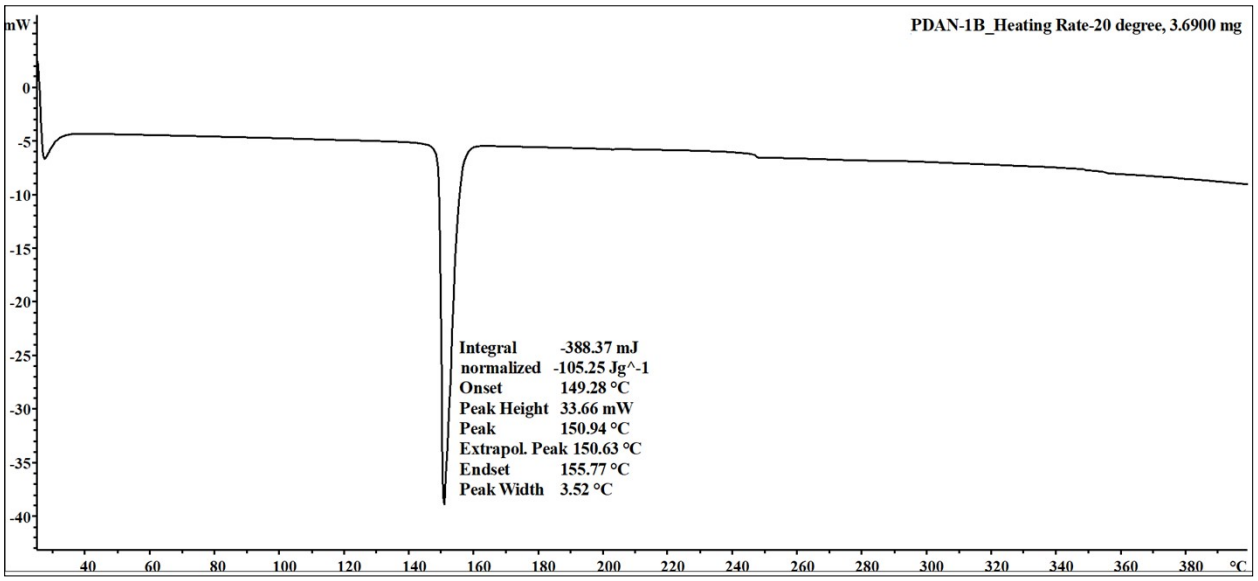
PDAN-1B_Heating Rate-20 degree, 3.6900 mg
mW
Integral -388.37 mJ
normalized -105.25 Jg^-1
Onset 149.28 °C
Peak Height 33.66 mW
Peak 150.94 °C
Extrapol. Peak 150.63 °C
Endset 155.77 °C
Peak Width 3.52 °C
°C

(c)

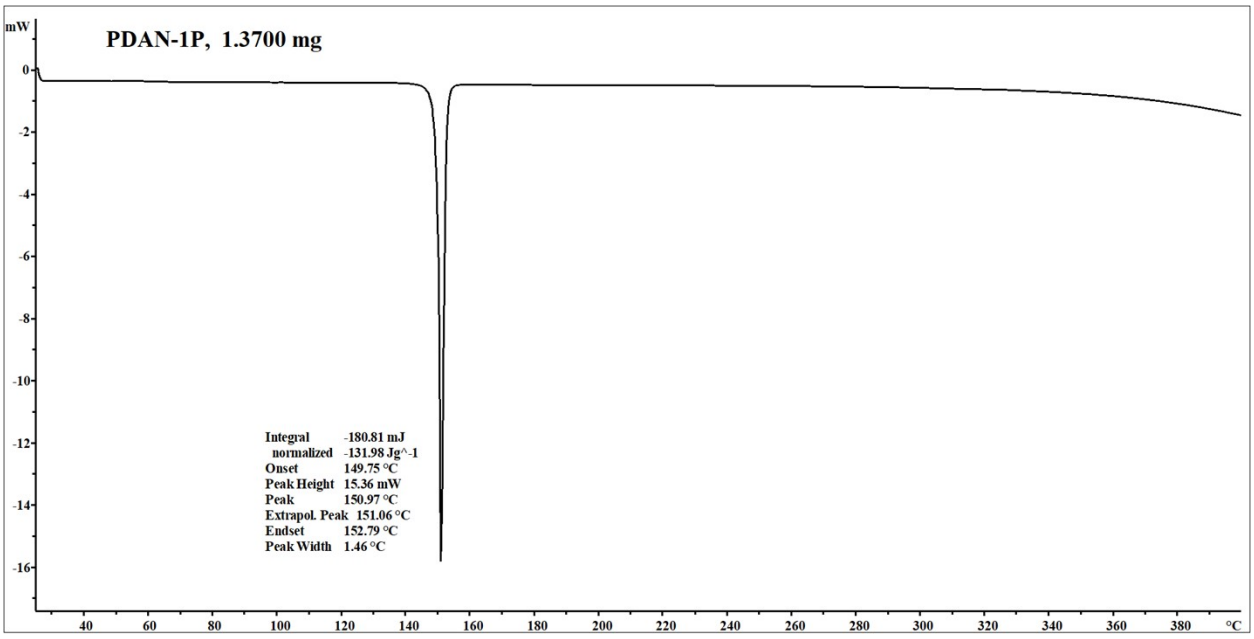

(d)

Figure S2. DSC thermogram of **PDAN-1B** at heating rate (a) 10 °C min^{-1}, (b) 5 °C min^{-1}, (c) 20 °C min^{-1} and (d) **PDAN-1P** form at a heating rate of 10 °C min^{-1}.

5. Phase purity analysis

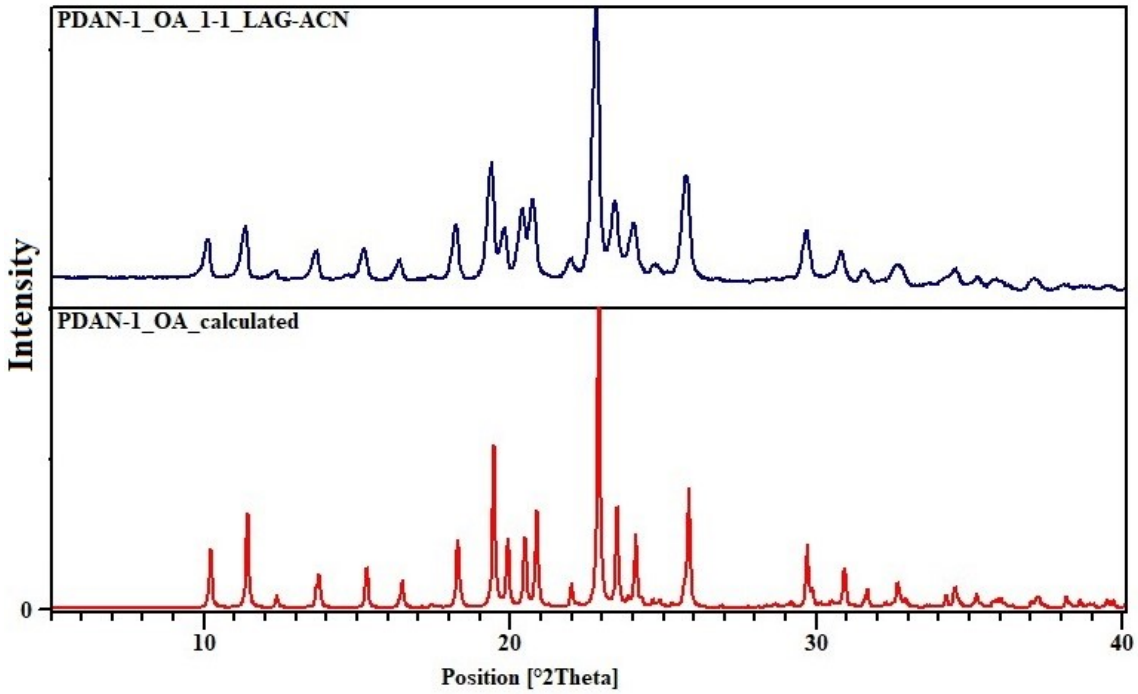

Figure S3. Comparison of calculated and experimental PXRD pattern of **PDAN-1•OA** salt cocrystal prepared using LAG with ACN.

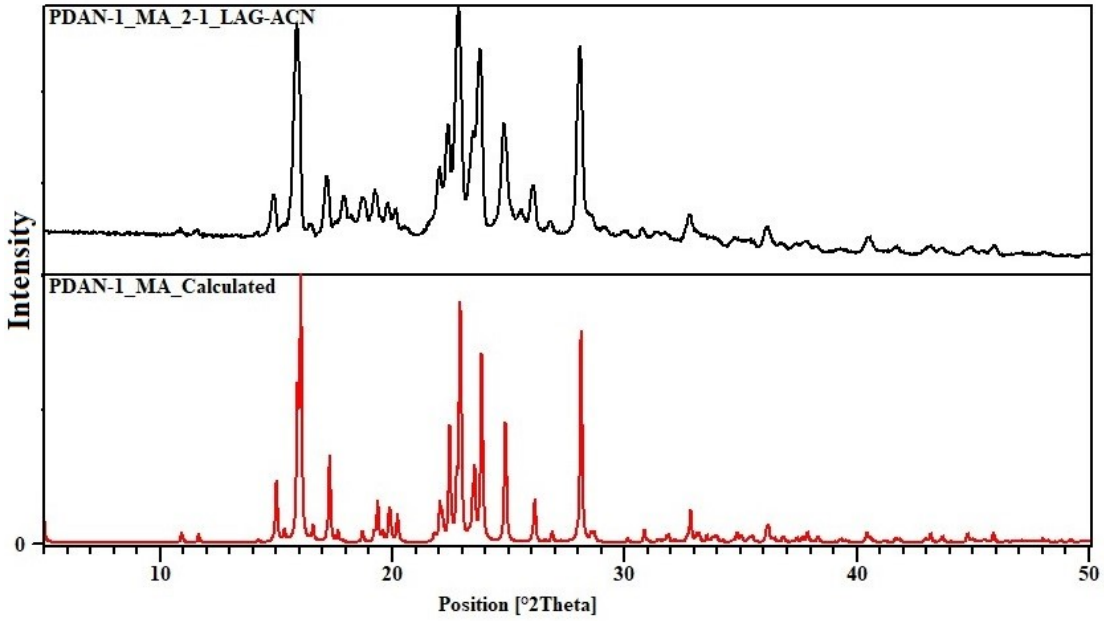

Figure S4. Comparison of calculated and experimental PXRD pattern of **PDAN-1•MA** cocrystal prepared using LAG with ACN.

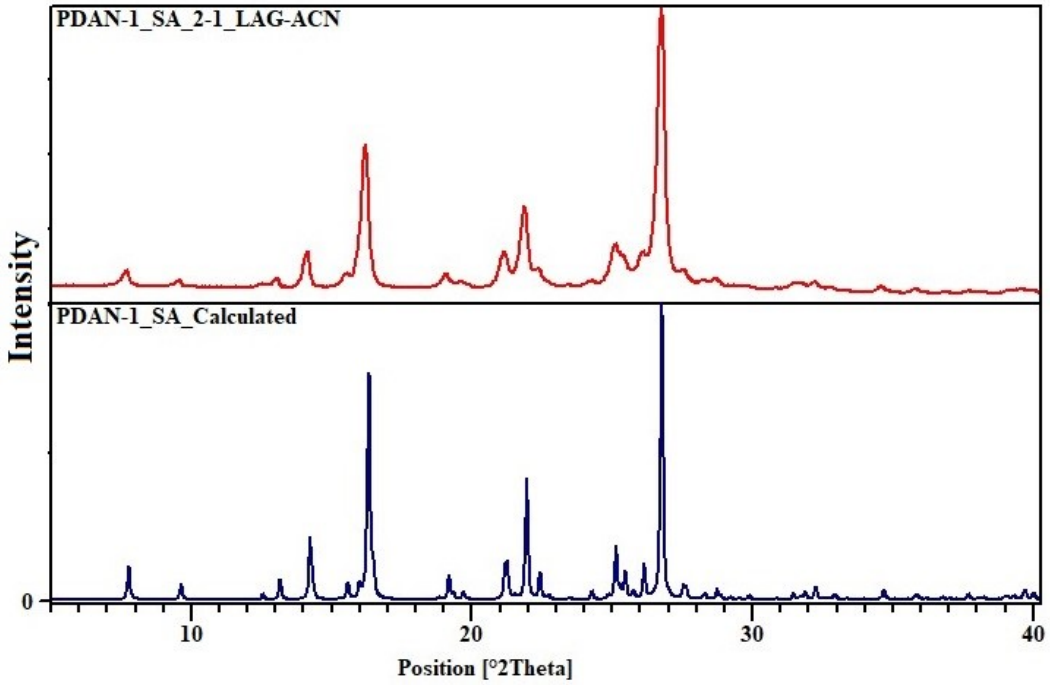

Figure S5. Comparison of calculated and experimental PXRD pattern of **PDAN-1•SA** cocrystal prepared using LAG with ACN.

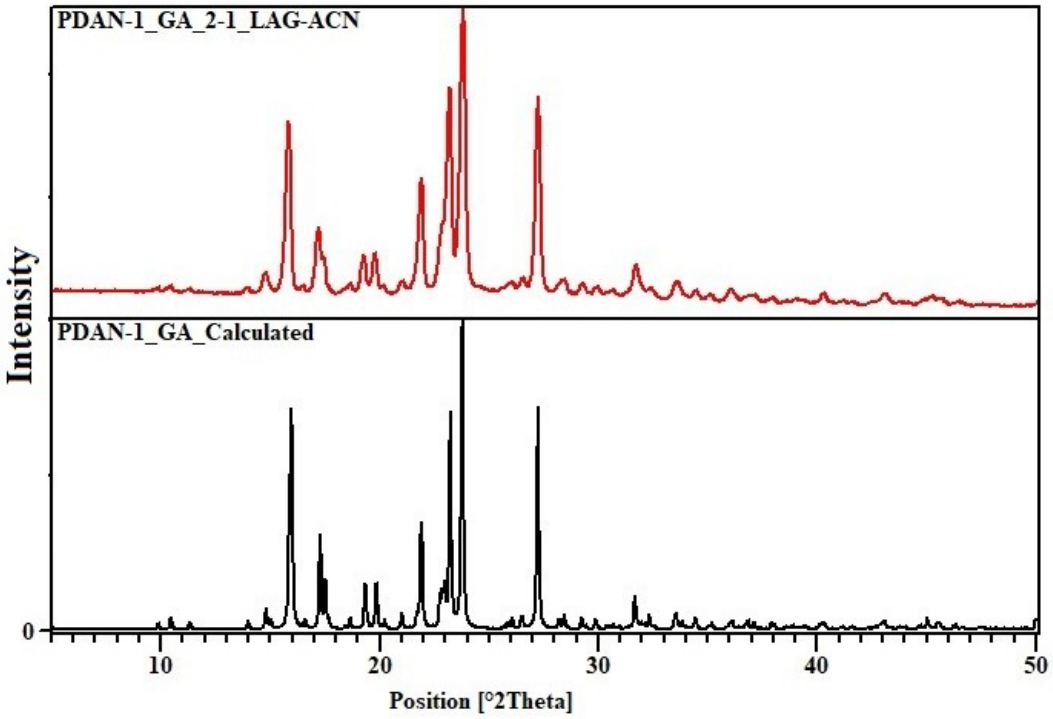

Figure S6. Comparison of calculated and experimental PXRD pattern of **PDAN-1•GA** cocrystal prepared using LAG with ACN.

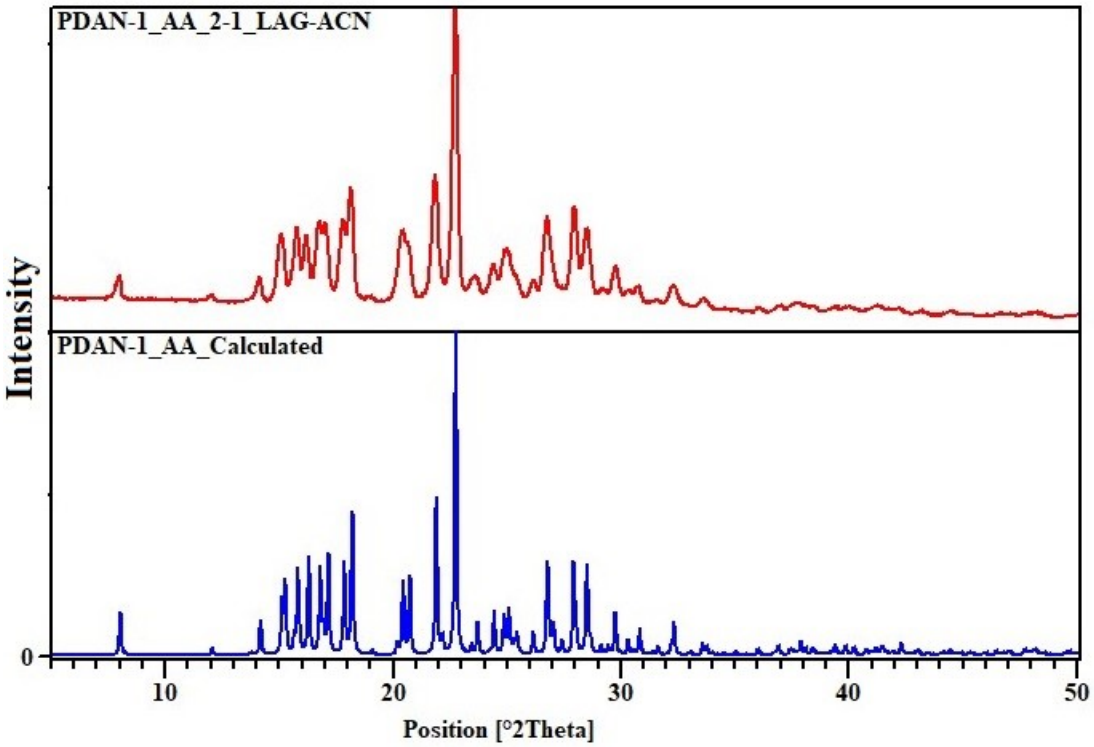

Figure S7. Comparison of calculated and experimental pxrd pattern of **PDAN-1•AA** cocrystal prepared using LAG with ACN.

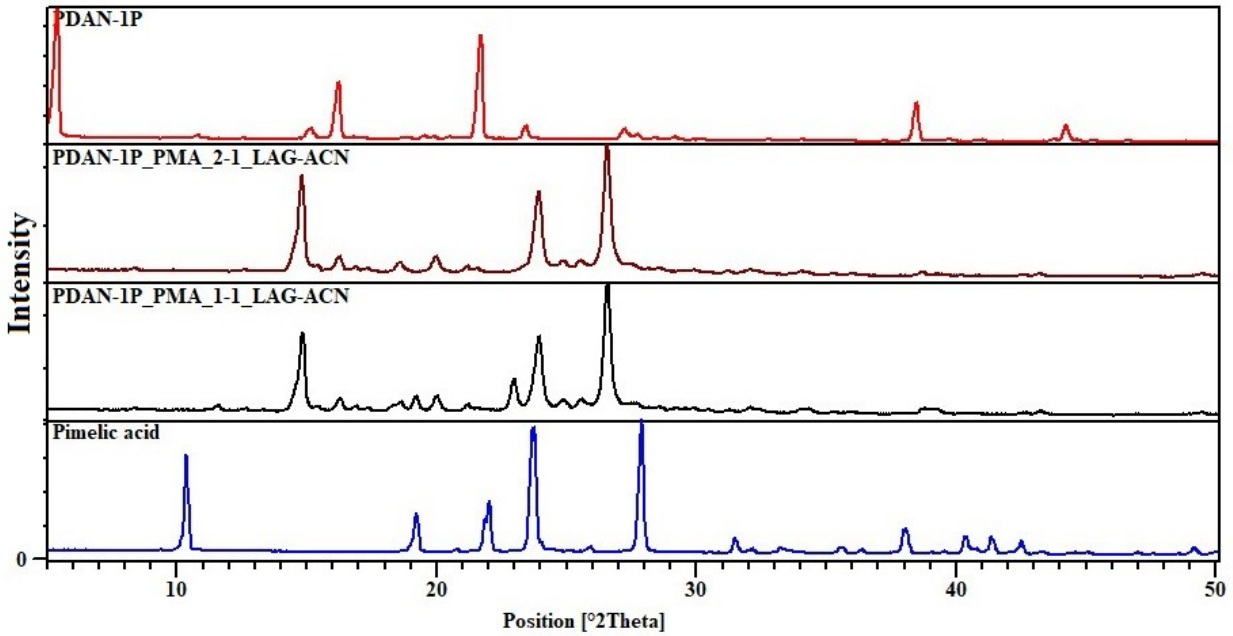

Figure S8. Comparison of PXRD pattern of **PDAN-1•PMA** with that of the starting materials.

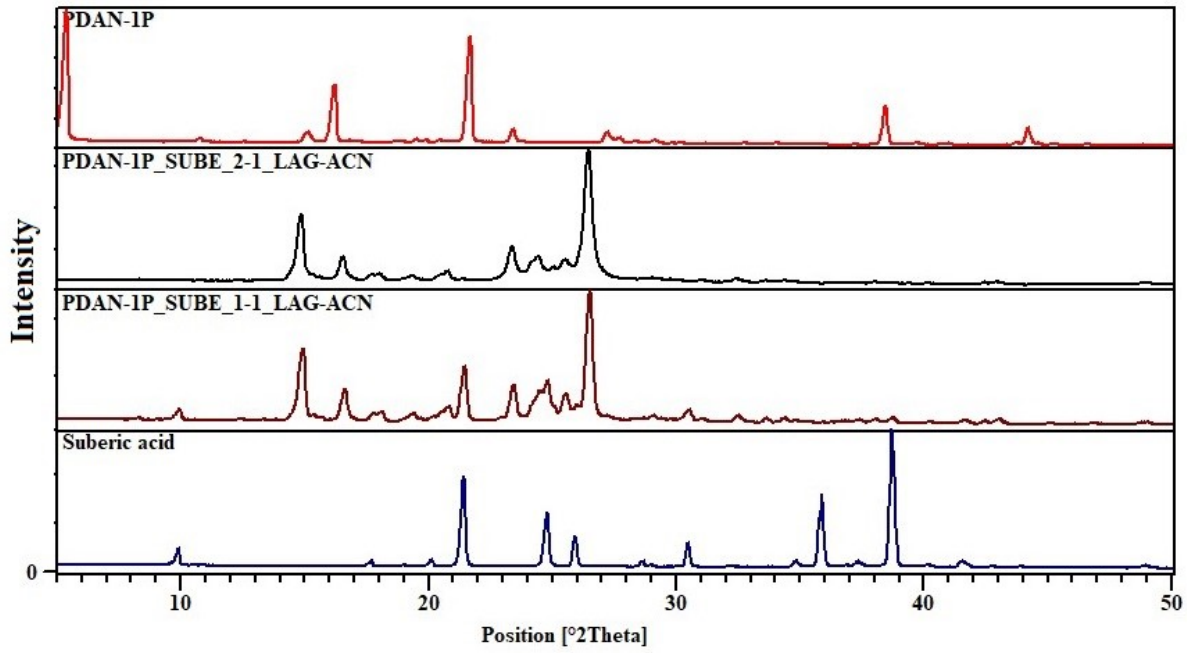

Figure S9. Comparison of PXRD pattern of **PDAN-1•SUBE** with that of the starting materials.

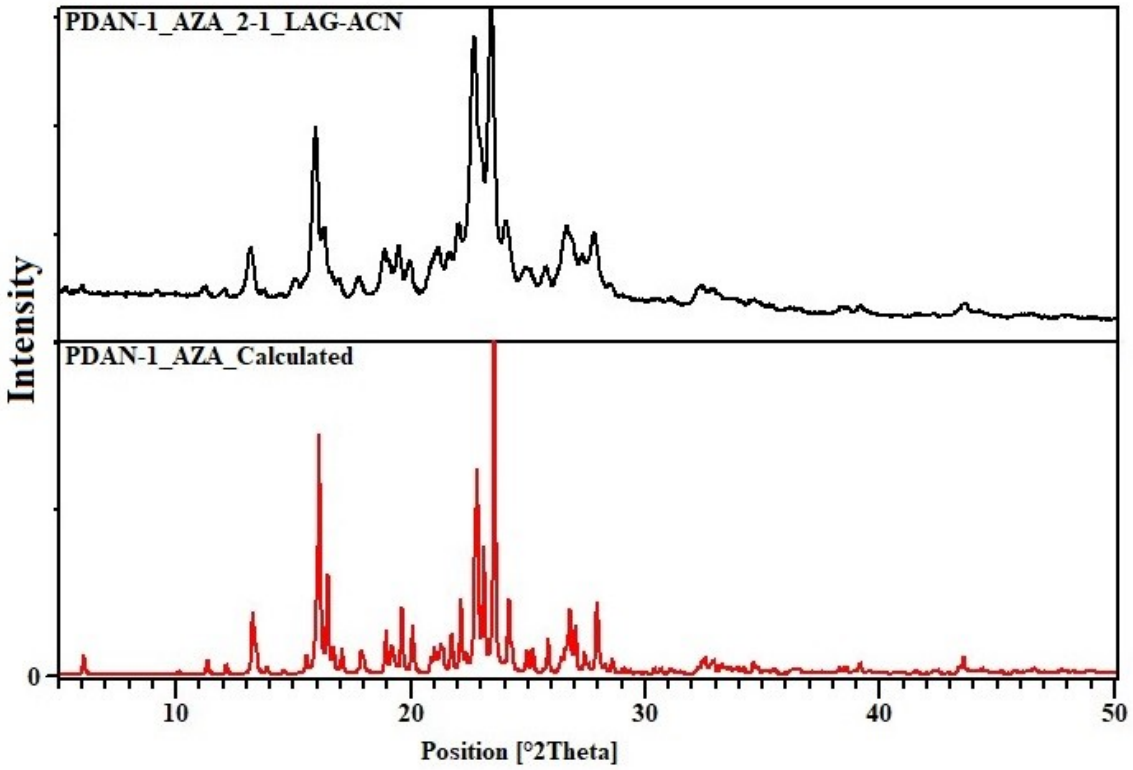

Figure S10. Comparison of calculated and experimental pxrd pattern of **PDAN-1•AZA** cocrystal prepared using LAG with ACN.

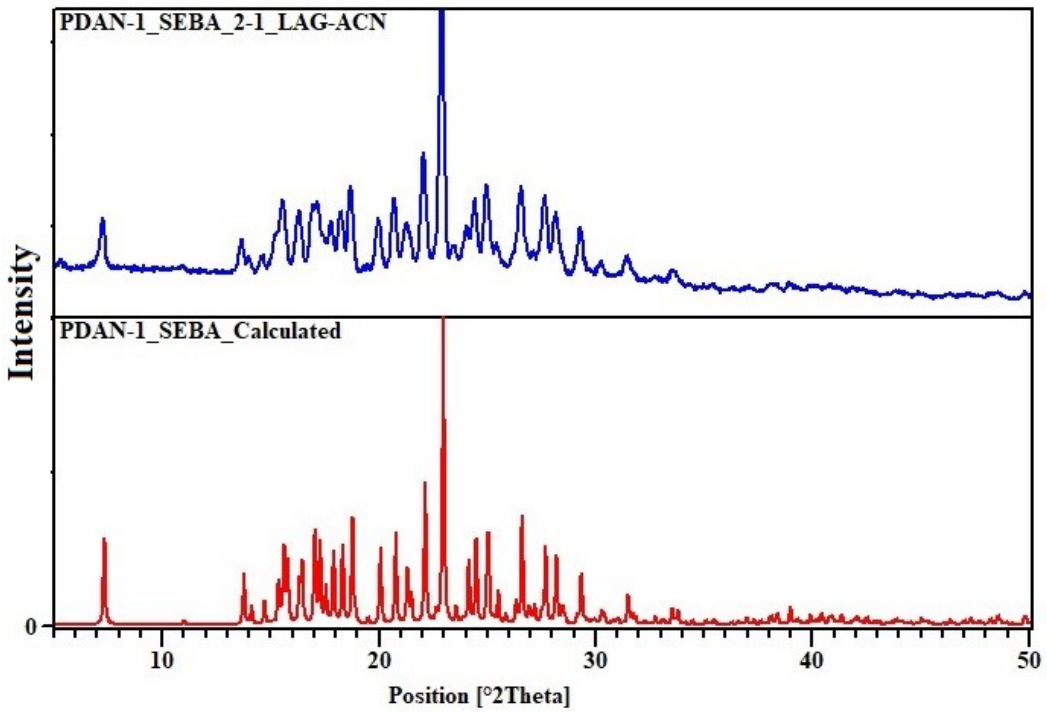

Figure S11. Comparison of calculated and experimental pxrd pattern of **PDAN-1•SEBA** cocrystal prepared using LAG with ACN.

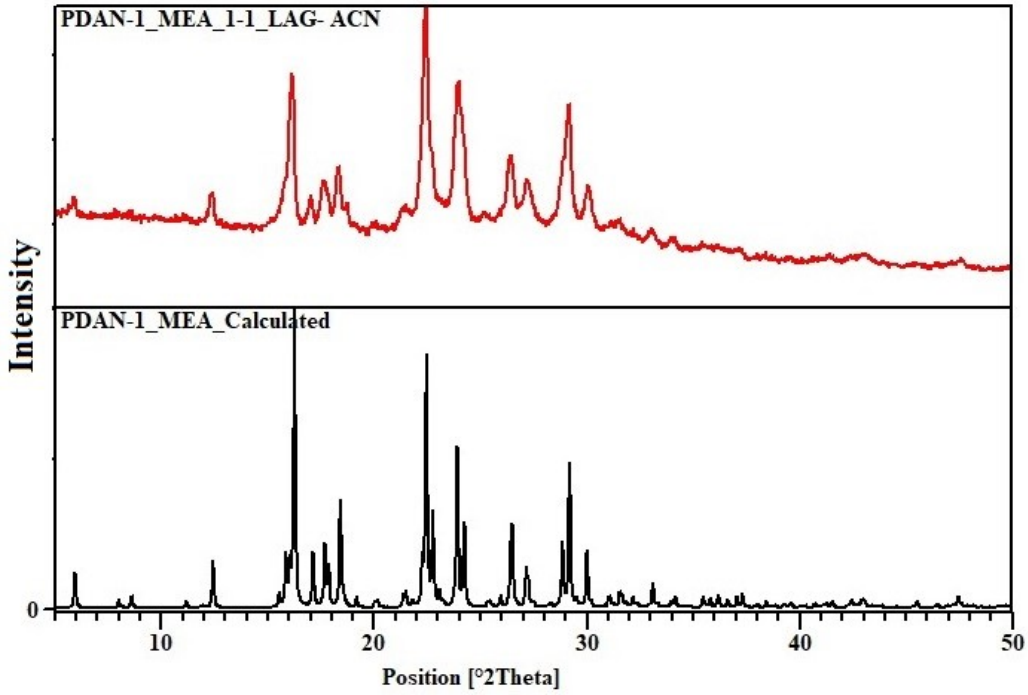

Figure S12. Comparison of calculated and experimental pxrd pattern of **PDAN-1•MEA** molecular salt prepared using LAG with ACN.

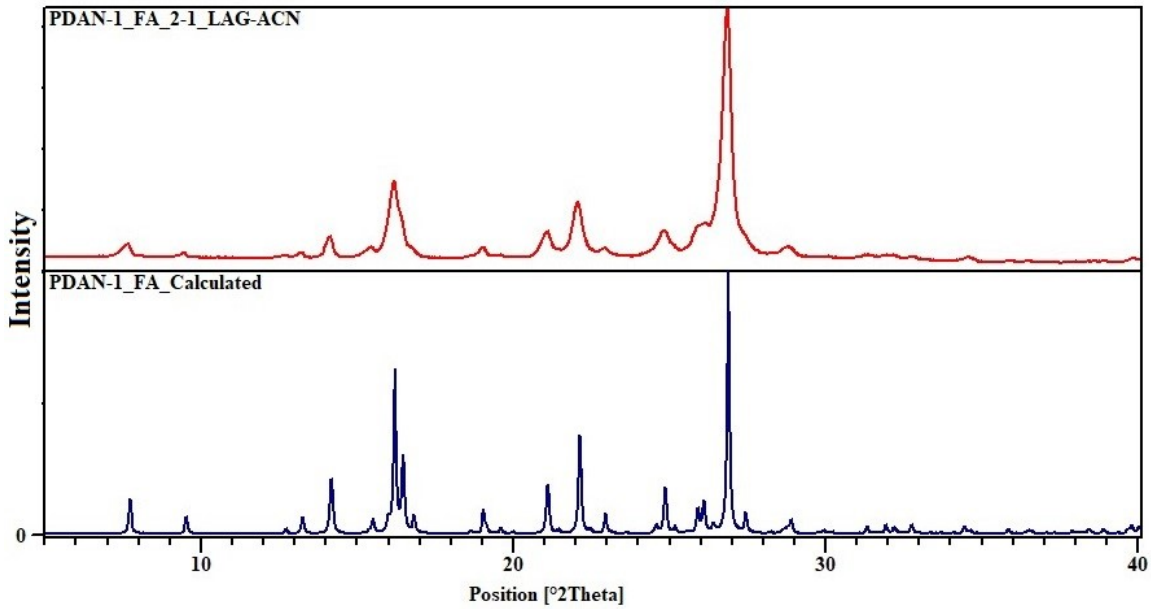

Figure S13. Comparison of calculated and experimental PXRD pattern of **PDAN-1•FA** cocrystal prepared using LAG with ACN.

6. Polymorph screening of all the PDAN-1 dicarboxylic acid cocrystals

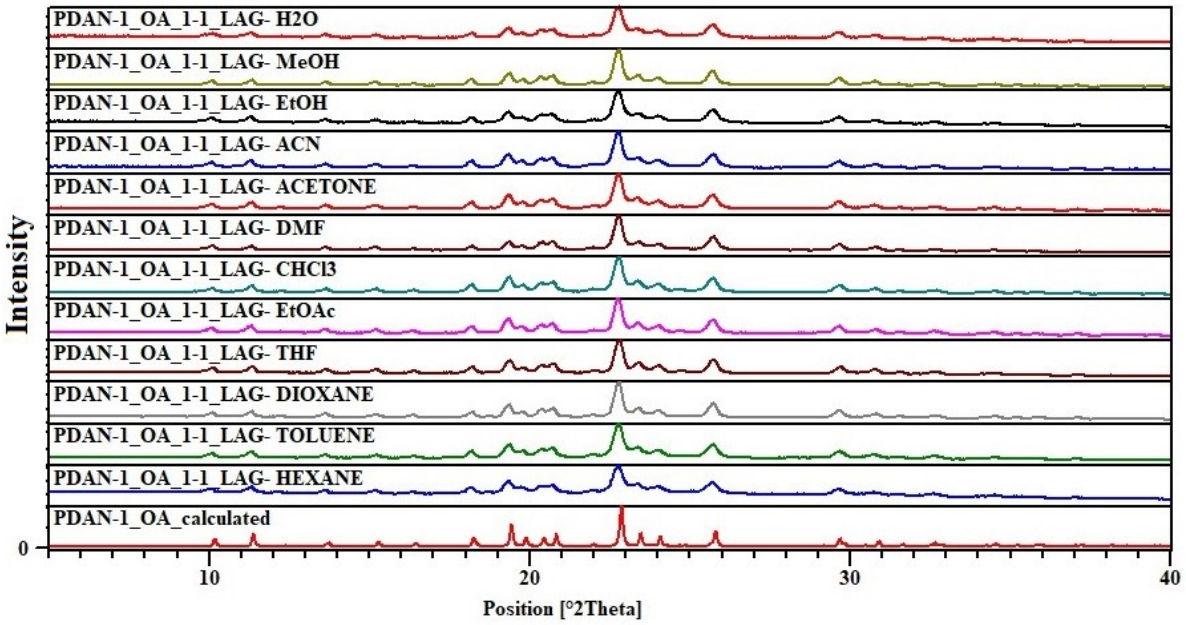

Figure S14. PXRD patterns of the ground materials of **PDAN-1•OA** using LAG with different liquids.

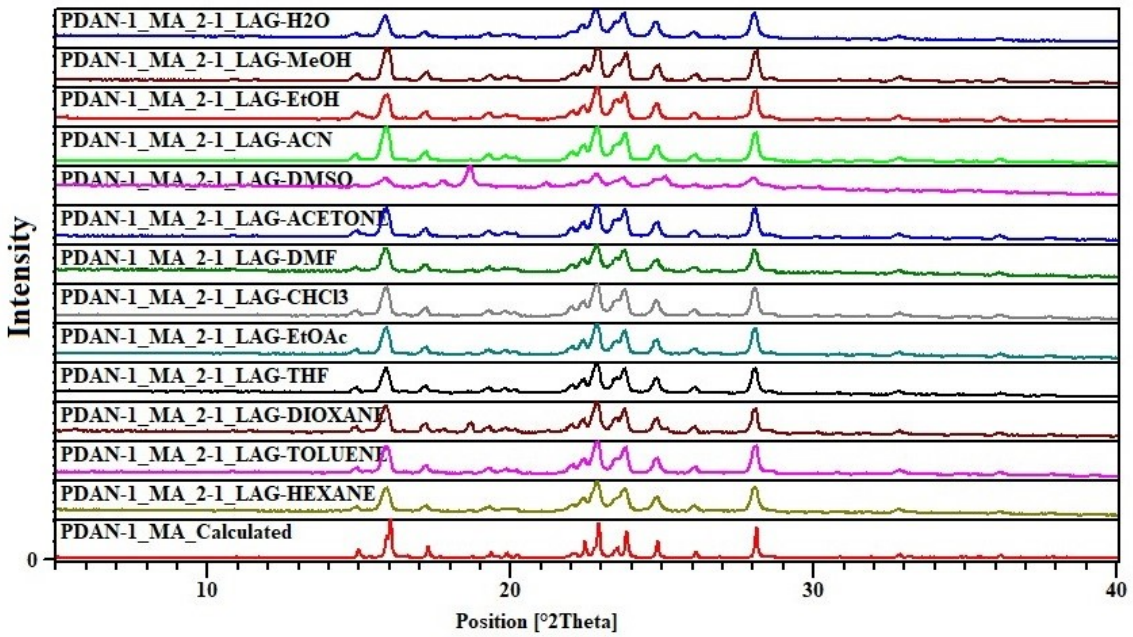

Figure S15. PXRD patterns of the ground materials of **PDAN-1•MA** using LAG with different liquids.

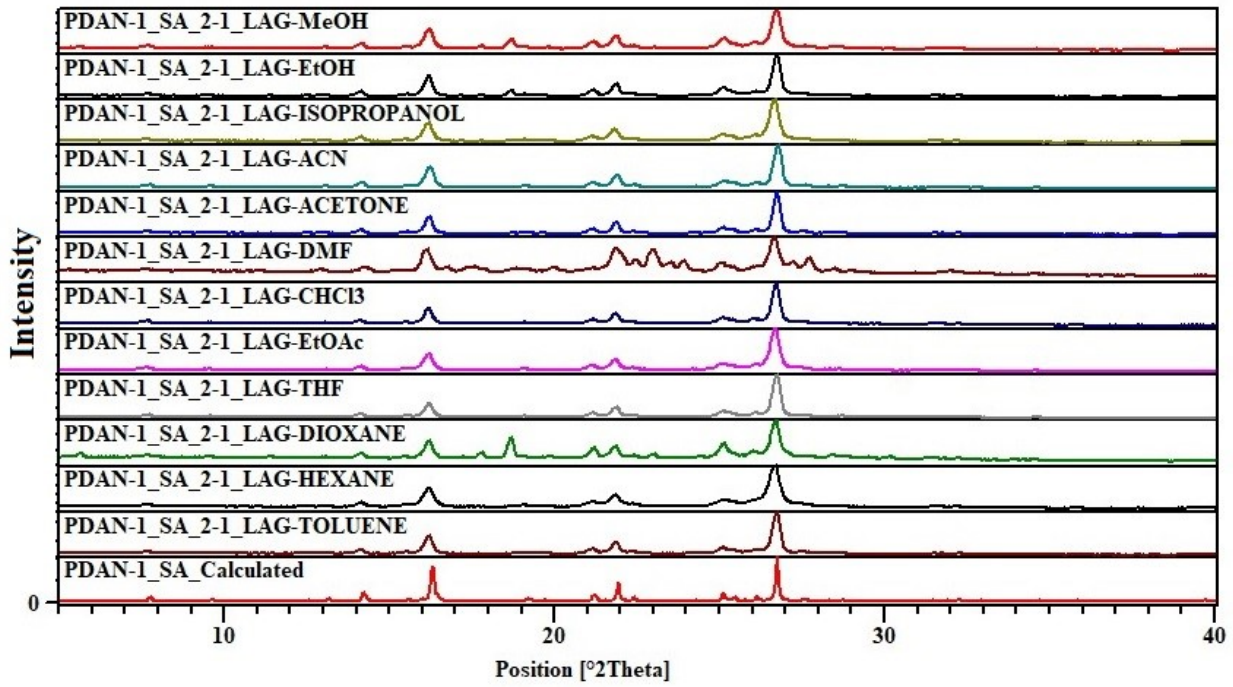

Figure S16. PXRD patterns of the ground materials of **PDAN-1•SA** using LAG with different liquids.

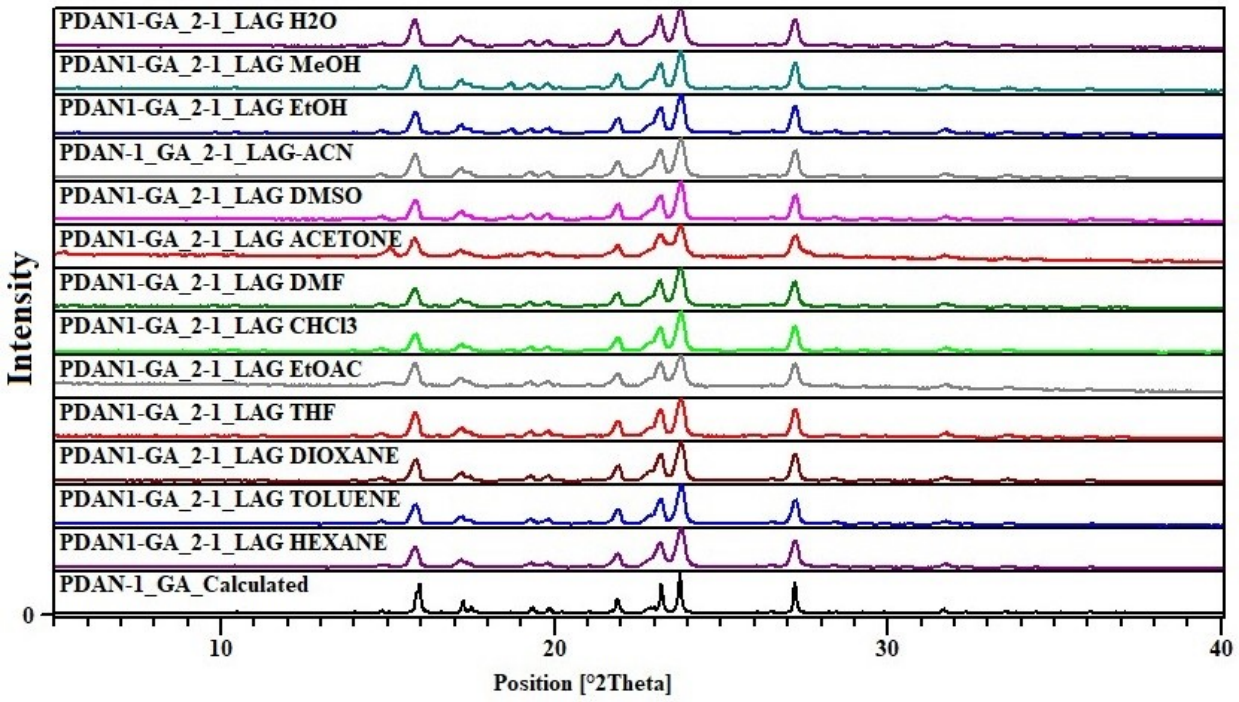

Figure S17. PXRD patterns of the ground materials of **PDAN-1•GA** using LAG with different liquids.

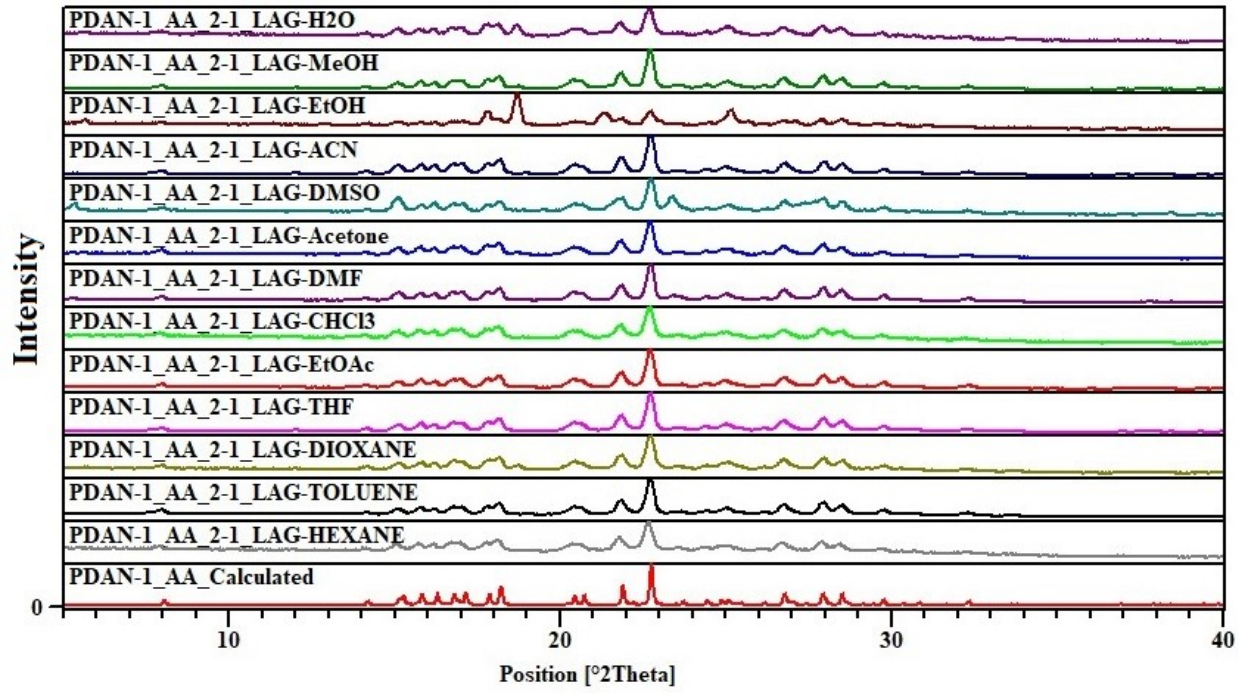

Figure S18. PXRD patterns of the ground materials of **PDAN-1•AA** using LAG with different liquids.

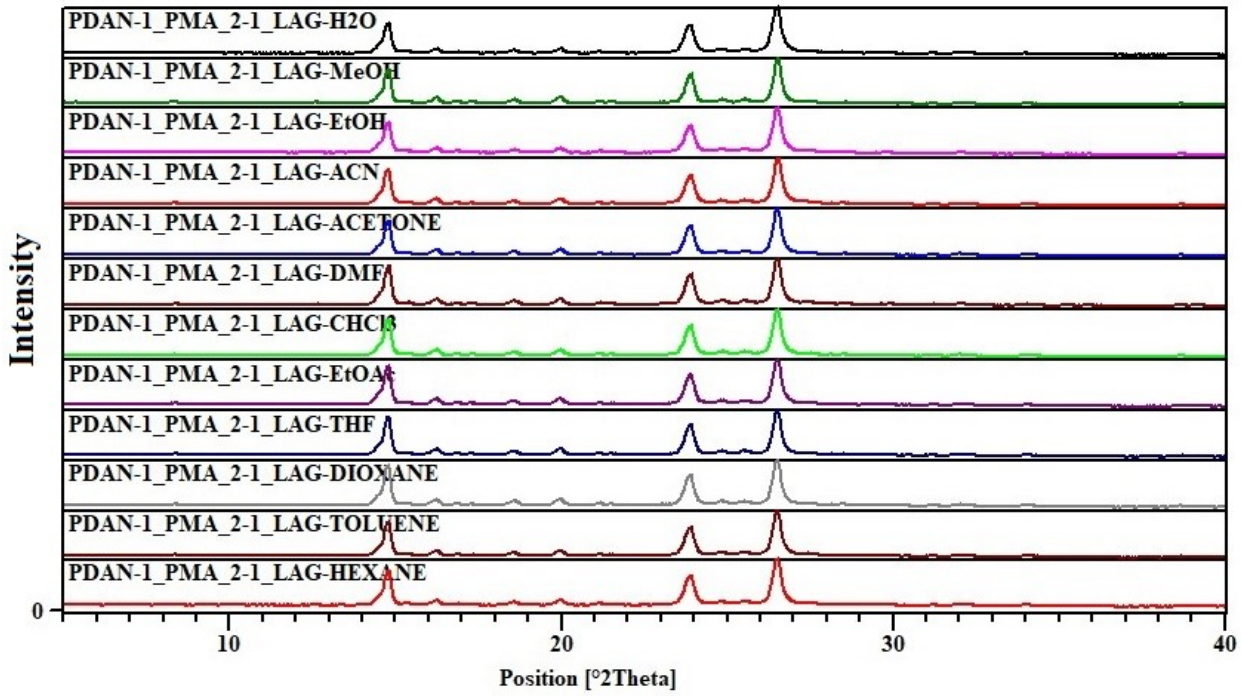

Figure S19. PXRD patterns of the ground materials of **PDAN-1•PMA** using LAG with different liquids.

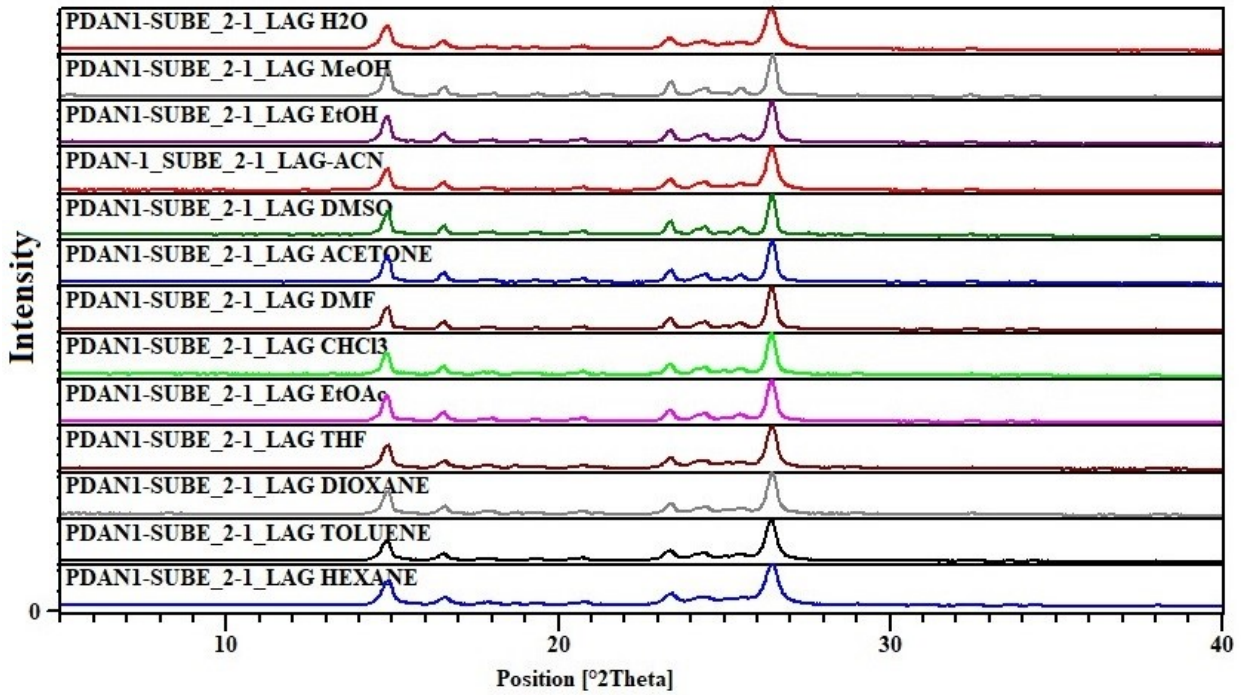

Figure S20. PXRD patterns of the ground materials of **PDAN-1•SUBE** using LAG with different liquids.

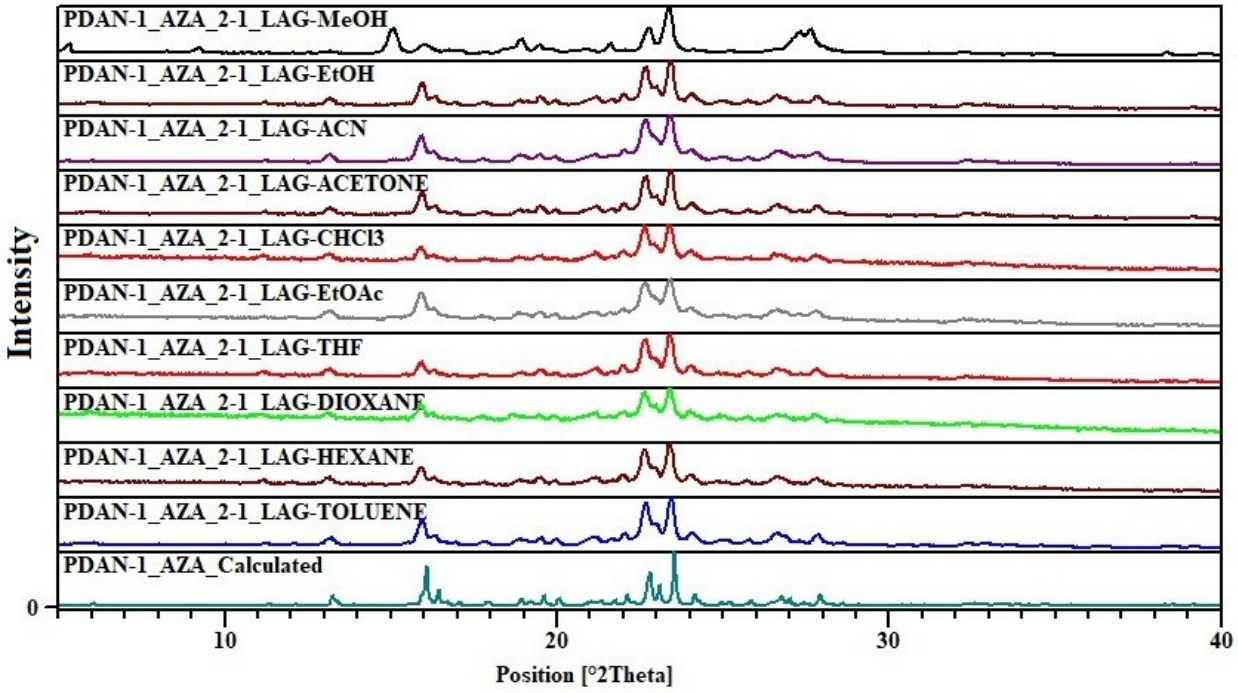

Figure S21. PXRD patterns of the ground materials of **PDAN-1•AZA** using LAG with different liquids.

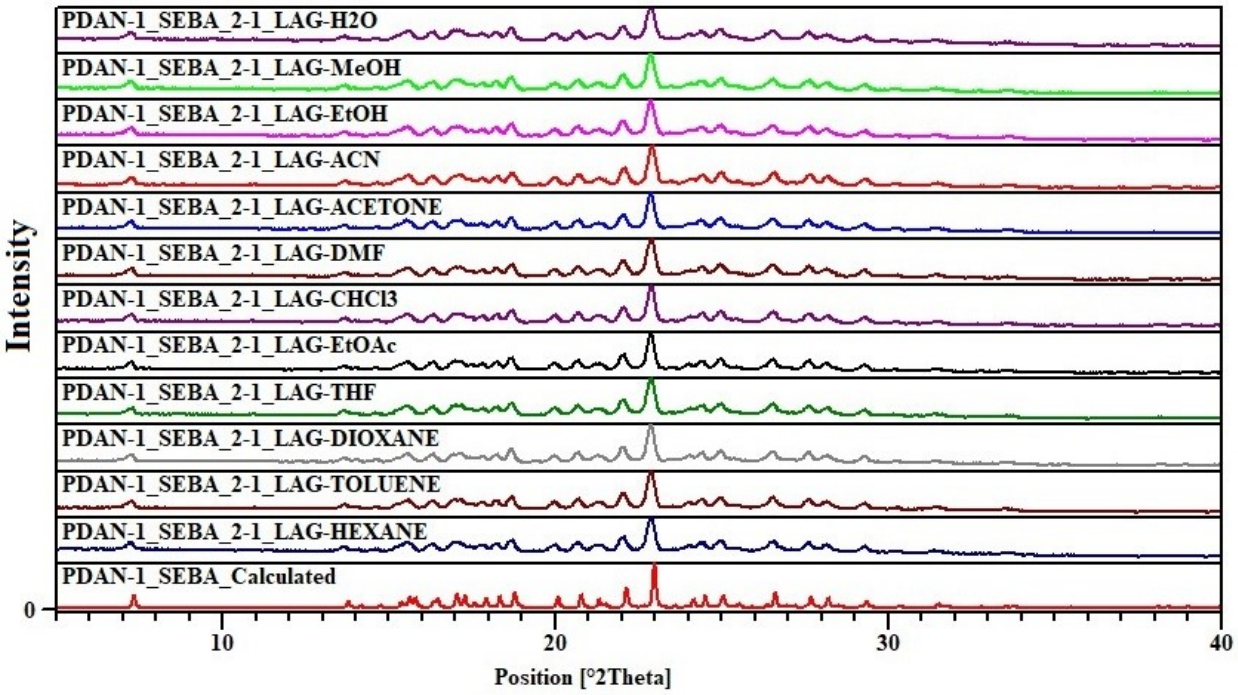

Figure S22. PXRD patterns of the ground materials of **PDAN-1•SEBA** using LAG with different liquids.

7. Table S1. Crystallographic parameters of **PDAN-1** and cocrystals/salts

	PDAN-1B	**PDAN-1P**	**PDAN-1P-Rigaku**
Chemical formula	$C_{20}H_{14}N_2$	$C_{20}H_{14}N_2$	$C_{20}H_{14}N_2$
M_r	282.33	282.33	282.33
Crystal system	Monoclinic	Triclinic	Triclinic
Space group	*Pc*	*P*1	*P*1
Temperature (K)	293	296	293
a (Å)	15.3938 (7)	6.05 (10)	5.9138 (13)
b (Å)	6.7893 (3)	7.73 (13)	7.5874 (9)
c (Å)	7.2409 (6)	17.2 (3)	16.538 (2)
α (°)	90	91.5 (4)	92.910 (12)
β (°)	90.158 (2)	98.6 (3)	97.60 (2)
γ (°)	90	92.4 (3)	92.256 (14)
V (Å^3)	756.77 (8)	793 (23)	733.8 (2)
Z	2	2	2
Radiation type	Mo *K*α	Mo Kα	Cu *K*α
μ (mm^{-1})	0.07	0.07	0.59
D_{calcd} (g cm^{-3})	1.239	1.182	1.278
Diffractometer	Bruker *APEX*-II CCD	Bruker APEX-II CCD	XtaLAB Synergy, Dualflex, HyPix
No. of measured reflections	6179	10928	7516
No. of observed [$I > 2\sigma(I)$] reflections	1601	2722	3073
R_{int}	0.085	0.130	0.130
$R[F^2 > 2\sigma(F^2)]$, ,	0.046	0.184	0.202
$wR(F^2)$	0.093	0.468	0.550
S	0.97	1.17	2.52
No. of reflections	2334	5727	3790
$\Delta\rho_{max}$(e Å^{-3})	0.12	0.70	1.08
CCDC No.	2393120	2393121	2441999

	PDAN-1•OA	**PDAN-1•MA**	**PDAN-1•SA**
Chemical formula	$C_{20}H_{15}N_2 \cdot 0.5(C_2H_2O_4) \cdot 0.5(C_2O_4)$	$2(C_{20}H_{14}N_2) \cdot C_3H_4O_4$	$C_{20}H_{14}N_2 \cdot 0.5(C_4H_6O_4)$
M_r	372.37	668.72	341.37

Crystal system	Triclinic	Monoclinic	Triclinic
Space group	$P\bar{1}$	*C*2/*c*	$P\bar{1}$
Temperature (K)	296	296	296
a (Å)	8.9403 (16)	35.665 (3)	6.8519 (12)
b (Å)	9.6410 (17)	5.9784 (5)	11.458 (2)
c (Å)	11.136 (2)	16.2082 (14)	11.848 (2)
α (°)	78.092 (4)	*90*	103.848 (4)
β (°)	81.505 (4)	94.387 (4)	96.792 (4)
γ (°)	77.354 (4)	90	97.046 (4)
V (Å^3)	911.1 (3)	3445.8 (5)	885.7 (3)
Z	2	4	2
Radiation type	Mo *K*α	Mo *K*α	Mo *K*α
μ (mm^{-1})	0.10	0.08	0.08
D_{calcd} (g cm^{-3})	1.357	1.289	1.280
Diffractometer	Bruker *APEX*-II CCD	Bruker *APEX*-II CCD	Bruker *APEX*-II CCD
No. of measured reflections	18380	33806	18333
No. of observed [$I > 2\sigma(I)$] reflections	3182	2804	3093
R_{int}	0.044	0.030	0.024
$R[F^2 > 2\sigma(F^2)]$, ,	0.037	0.041	0.041
$wR(F^2)$	0.114	0.129	0.129
S	0.94	0.96	0.99
No. of reflections	3707	3549	3610
$\Delta\rho_{max}$(e Å^{-3})	0.15	0.14	0.24
CCDC No.	2393122	2393127	2393126

	PDAN-1•GA	**PDAN-1•AA**	**PDAN-1•AZA**
Chemical formula	$2(C_{20}H_{14}N_2)\cdot C_5H_8O_4$	$C_{20}H_{14}N_2\cdot 0.5(C_6H_{10}O_4)$	$2(C_{20}H_{14}N_2)\bullet C_9H_{16}O_4$
M_r	696.78	355.40	752.88
Crystal system	Monoclinic	Monoclinic	Monoclinic
Space group	*C*2/*c*	$P2_1/n$	$P2_1/c$
Temperature (K)	296	296	296
a (Å)	35.879 (5)	6.6656 (9)	43.708 (7)
b (Å)	5.9716 (8)	43.969 (6)	8.3458 (13)
c (Å)	16.917 (3)	7.2128 (10)	11.0983 (17)
α (°)	*90*	*90*	*90*

β (°)	93.199 (4)	115.616 (3)	90.164 (4)
γ (°)	90	90	90
V (Å^3)	3618.9 (9)	1906.1 (5)	4048.4 (11)
Z	4	4	4
Radiation type	Mo $K\alpha$	Mo $K\alpha$	Mo $K\alpha$
μ (mm^{-1})	0.08	0.08	0.08
D_{calcd} (g cm^{-3})	1.279	1.238	1.235
Diffractometer	Bruker *APEX*-II CCD	Bruker *APEX*-II CCD	Bruker *APEX*-II CCD
No. of measured reflections	34478	26092	53812
No. of observed [$I > 2\sigma(I)$] reflections	3575	4030	6410
R_{int}	0.041	0.047	0.062
$R[F^2 > 2\sigma(F^2)]$, ,	0.052	0.064	0.062
$wR(F^2)$	0.190	0.185	0.212
S	0.98	1.01	1.00
No. of reflections	5345	5831	12403
$\Delta\rho_{max}$(e Å^{-3})	0.21	0.21	0.30
CCDC No.	2393128	2393124	2393129

	PDAN-1•SEBA	**PDAN-1•MEA**	**PDAN-1•FA**
Chemical formula	$C_{20}H_{14}N_2 \cdot 0.5(C_{10}H_{18}O_4)$	$C_{20}H_{15}N_2 \bullet C_4H_3O_4$	$C_{20}H_{15}N_2 \bullet 0.5(C_4H_2O_4)$
M_r	383.45	398.40	340.37
Crystal system	Monoclinic	Monoclinic	Triclinic
Space group	$P2_1/n$	$P2_1/c$	$P\bar{1}$
Temperature (K)	296	293	296
a (Å)	6.6460 (16)	30.897 (3)	6.842 (3)
b (Å)	48.219 (11)	11.6158 (12)	11.415 (4)
c (Å)	7.1154 (16)	22.946 (2)	11.977 (4)
α (°)	90	90	104.802 (8)
β (°)	114.288 (4)	105.539 (3)	97.205 (9)
γ (°)	90	90	98.435 (8)
V (Å^3)	2078.4 (8)	7934.2 (13)	881.5 (6)
Z	4	16	2
Radiation type	Mo $K\alpha$	Mo $K\alpha$	Mo $K\alpha$
μ (mm^{-1})	0.08	0.09	0.08
D_{calcd} (g cm^{-3})	1.225	1.334	1.282

Diffractometer	Bruker *APEX*-II CCD	Bruker *APEX*-II CCD	Bruker *APEX*-II CCD
No. of measured reflections	18702	162323	16192
No. of observed [$I > 2\sigma(I)$] reflections	4698	8094	3048
R_{int}	0.042	0.050	0.042
$R[F^2 > 2\sigma(F^2)]$, ,	0.071	0.078	0.057
$wR(F^2)$	0.207	0.277	0.156
S	1.05	1.04	1.03
No. of reflections	6206	16470	5388
$\Delta\rho_{max}$(e Å^{-3})	0.31	0.48	0.20
CCDC No.	2393123	2393130	2393125

8. Photo-physical property of synthesized cocrystals/salts

UV-vis Spectra

The UV-Vissible spectra of all the synthesized cocrystals are recorded which give absorbance peaks at around 337-340 nm (Figure S23).

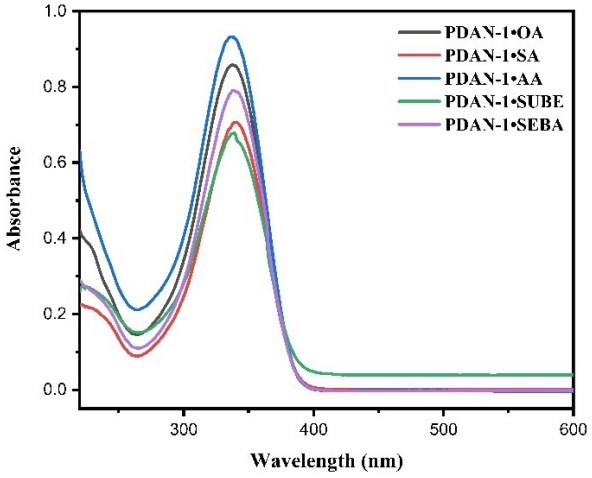

(a)

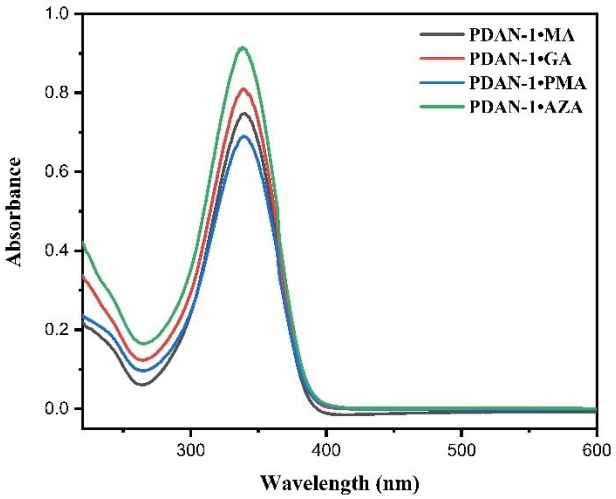

(b)

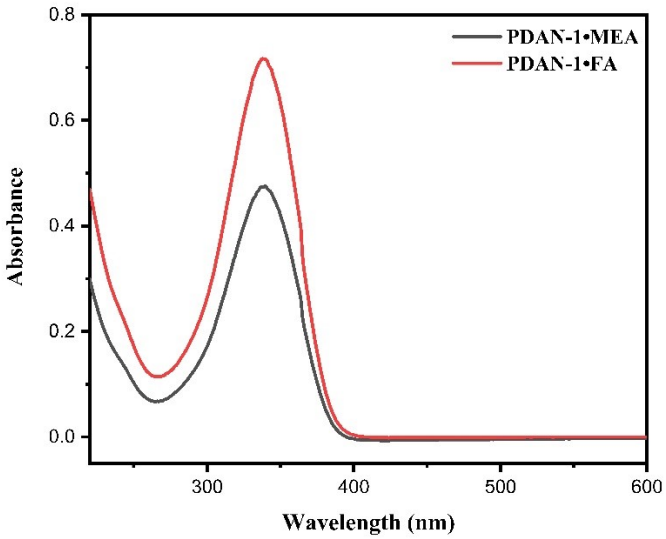

(c)

Figure S23. The solution-state uv-vissible spectra of (a) **PDAN-1** with even diacids viz. **PDAN-1•OA**, **PDAN-1•SA**, **PDAN-1•AA**, **PDAN-1•SUBE** and **PDAN-1•SEBA**; (b) **PDAN-1** with odd diacids viz. **PDAN-1•MA**, **PDAN-1•GA**, **PDAN-1•PMA** and **PDAN-1•AZA**; (c) **PDAN-1•MEA** and **PDAN-1•FA** cocrystals.

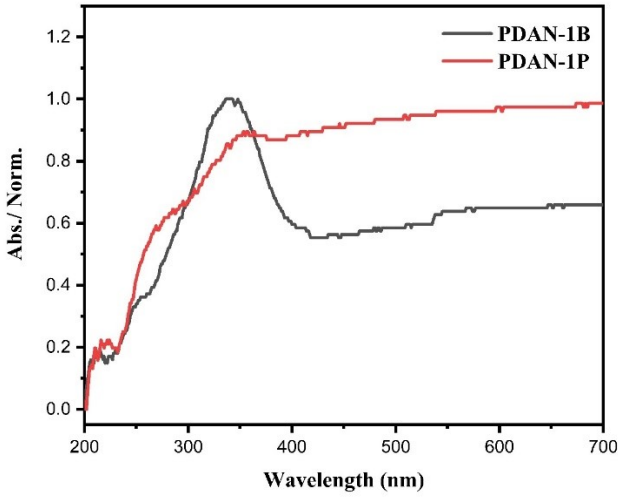

(a)

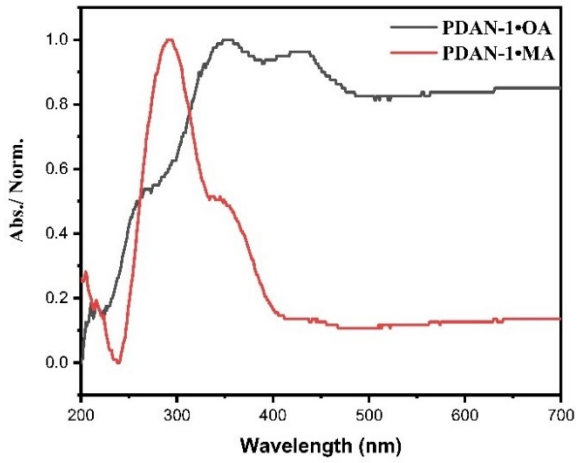
PDAN-1•OA
PDAN-1•MA
Abs./ Norm.
Wavelength (nm)

(b)

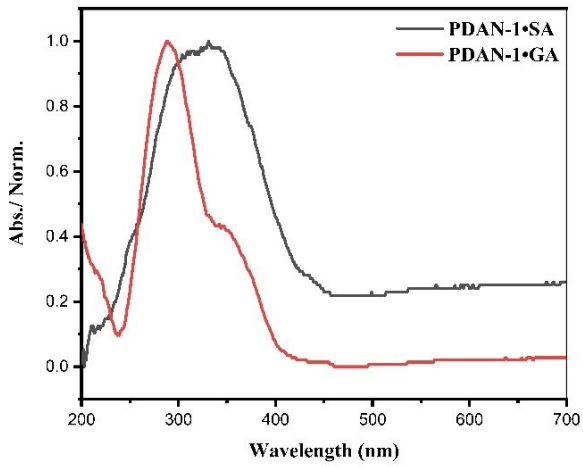
PDAN-1•SA
PDAN-1•GA
Abs./ Norm.
Wavelength (nm)

(c)

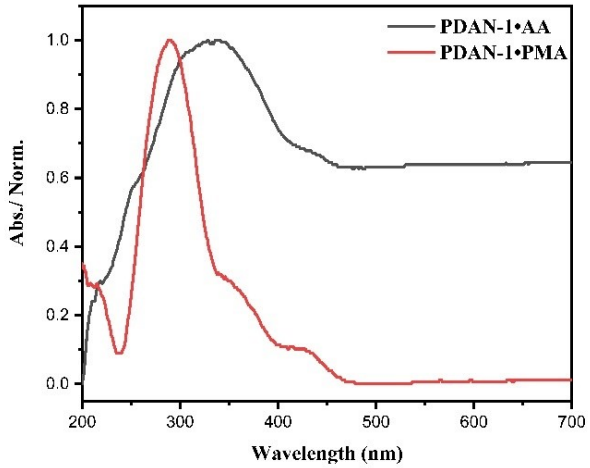
PDAN-1•AA
PDAN-1•PMA
Abs./ Norm.
Wavelength (nm)

(d)

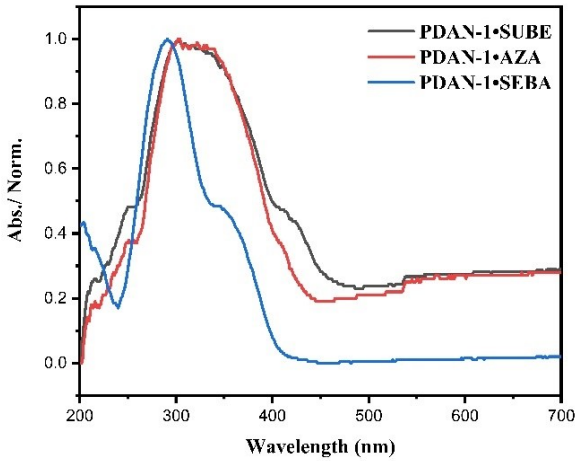
PDAN-1•SUBE
PDAN-1•AZA
PDAN-1•SEBA
Abs./ Norm.
Wavelength (nm)

(e)

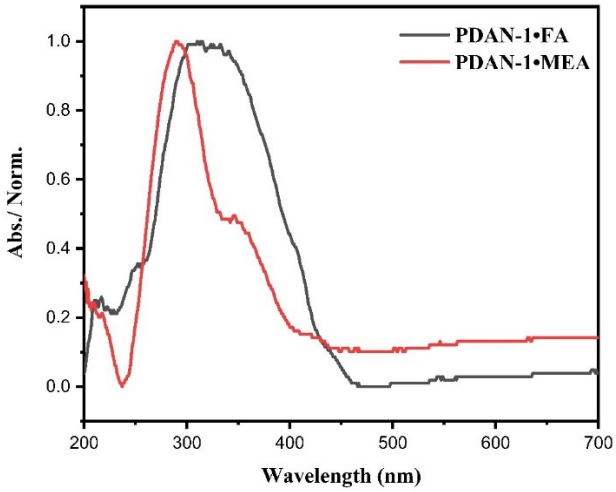
PDAN-1•FA
PDAN-1•MEA
Abs./ Norm.
Wavelength (nm)

(f)

Figure S24. The solid-state uv-vissible spectra of (a) **PDAN-1B** and **PDAN-1P**; (b) **PDAN-1•OA** and **PDAN-1•MA**; (c) **PDAN-1•SA** and **PDAN-1•GA**; (d) **PDAN-1•AA** and **PDAN-1•PMA**; (e) **PDAN-1•SUBE**, **PDAN-1•AZA** and **PDAN-1•SEBA**; (f) **PDAN-1•MEA** and **PDAN-1•FA**.

Fluorescence Spectra

Solid-state fluorescence spectra of all the cocrystals are recorded at an excitation wavelength of 365 nm. The fluorescence spectra of the cocrystals having diacids with even numbered C-atoms give an emission in blue region with an emission center at around 400-450 nm except for C_8 (gives a cyan emission). On the other hand, the cocrystals having diacids with odd numbered C-atoms has an emission in comparatively longer wavelength region (470-500 nm) giving cyan color (C_9 is an exception with blue color) (Figure S25).

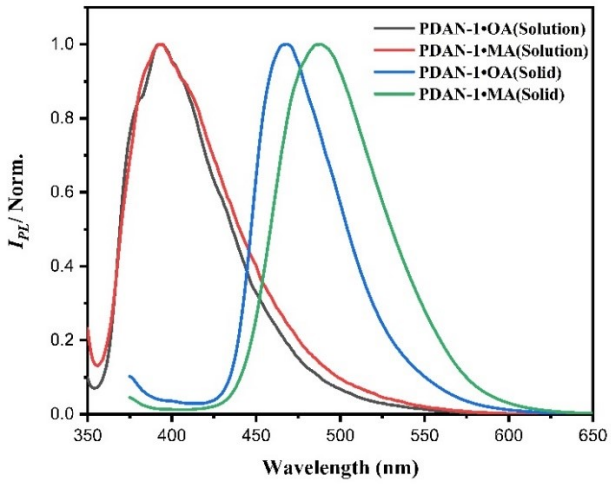

(a)

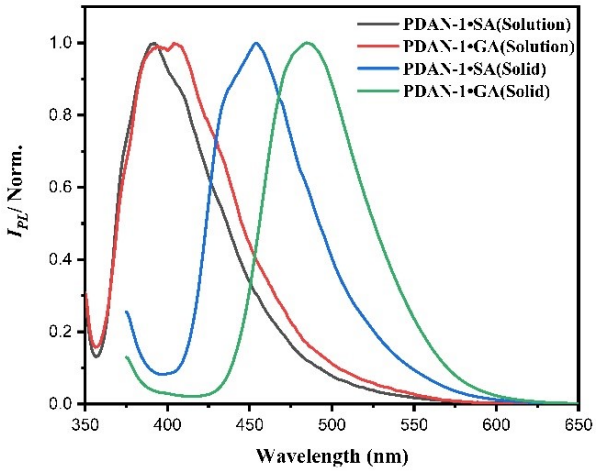

(b)

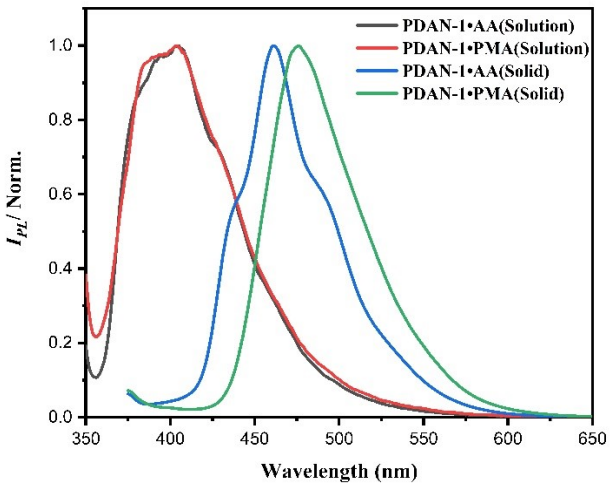

(c)

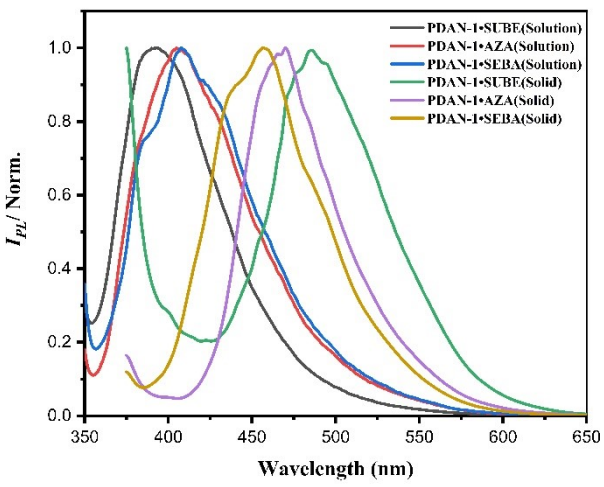

(d)

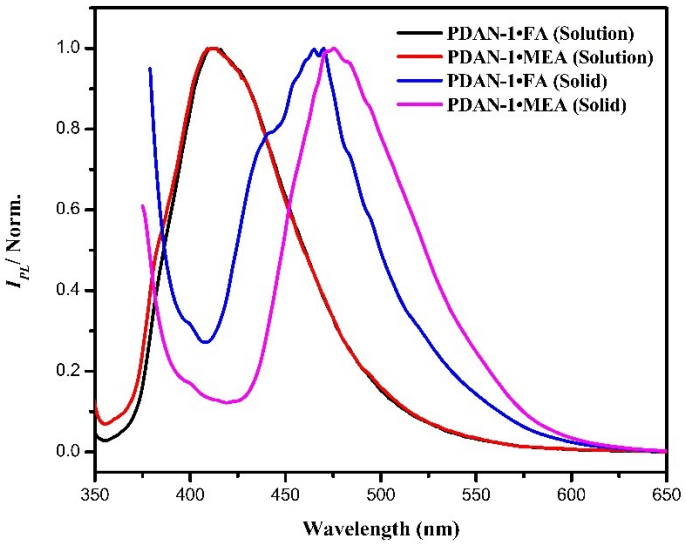

(e)

Figure S25. Solution and solid-state fluorescence spectra of (a) **PDAN-1•OA** and **PDAN-1•MA;** (b) **PDAN-1•SA** and **PDAN-1•GA**; (c) **PDAN-1•AA** and **PDAN-1•PMA**; (d) **PDAN-1•SUBE**, **PDAN-1•AZA** and **PDAN-1•SEBA**; and (e) **PDAN-1•MEA** and **PDAN-1•FA** at an excitation wavelength of 365 nm.

The alternation of solid-state fluorescence of **PDAN-1** diacids based on odd-even parity can be better represented by CIE chromaticity diagram that shows two different regions of color for the odd and even diacid cocrystals of **PDAN-1** (Figure S26).

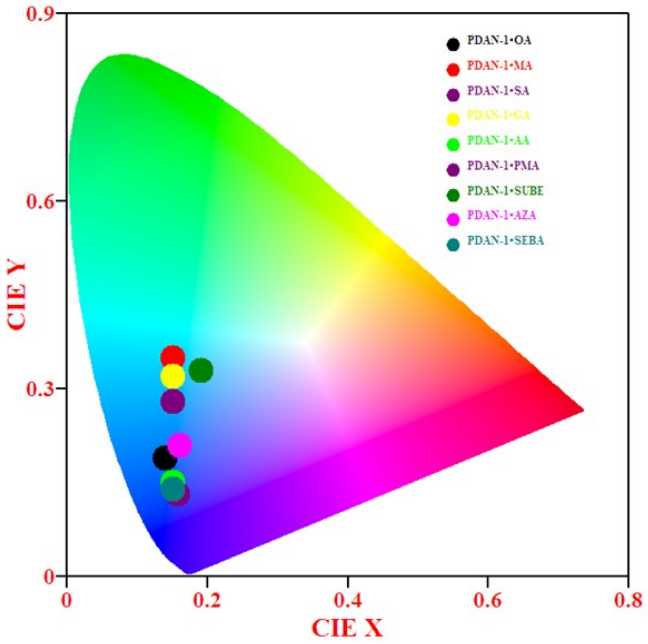

Figure S26. CIE chromaticity diagram for **PDAN-1•**diacid cocrystals.

9. Photoluminescence (PL) decay study

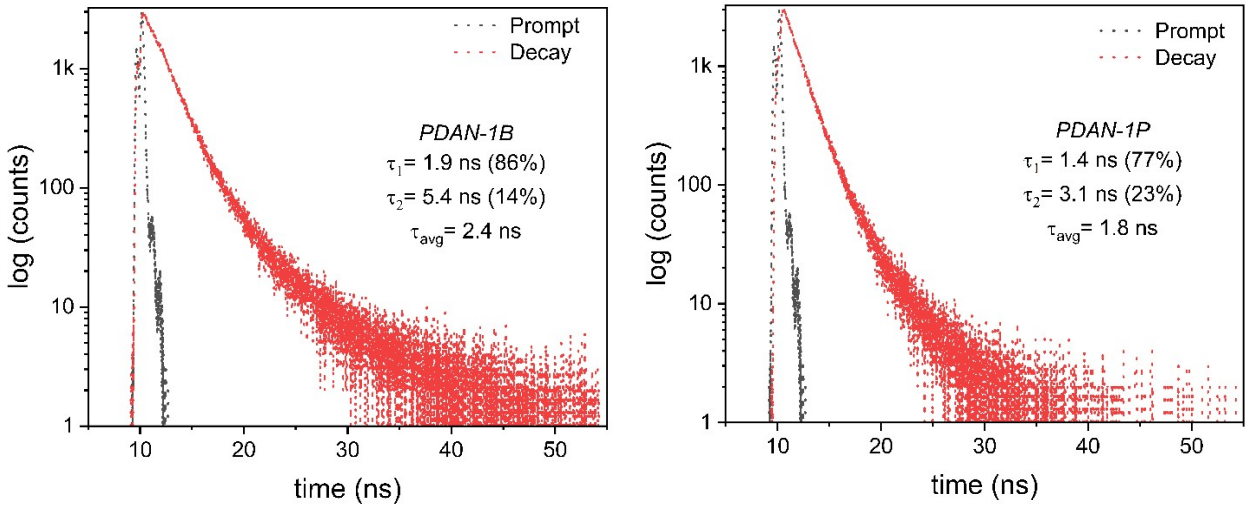

(a) (b)

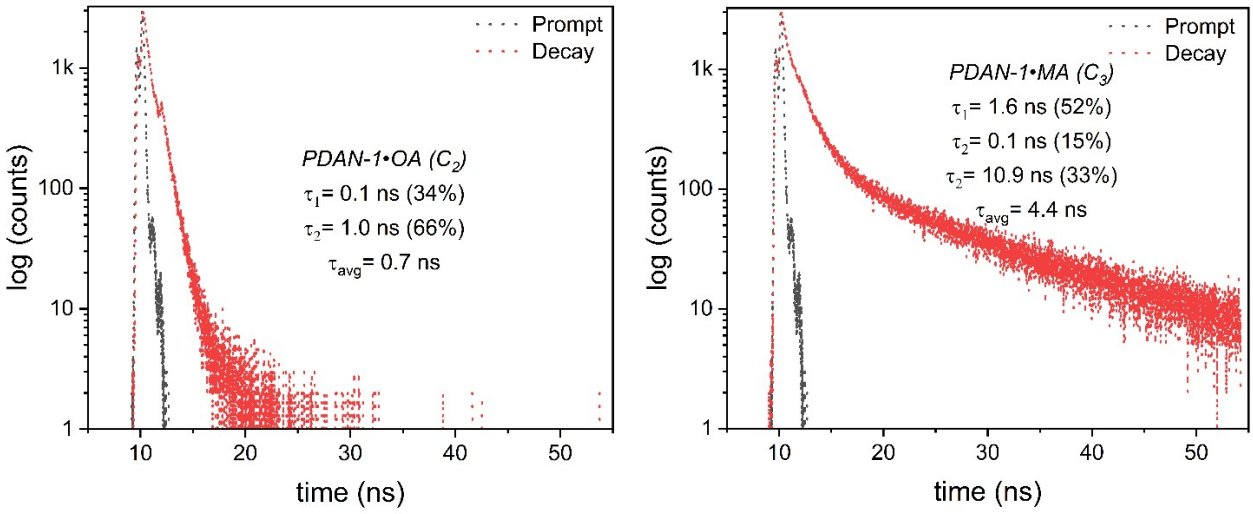

(c) (d)

Figure S27. Lifetime decay profile of (a) **PDAN-1B**, (b) **PDAN-1P**, (c) **PDAN-1•OA** and (d) **PDAN-1•MA** respectively. All the samples were excited using a 371 nm LASER. Emissions were collected at the respective emission maximum.

10. Aggregation Induced Titration

To investigate the AIE behaviour of the synthesized cocrystals, we performed aggregation induced titration for all the cocrystals in ethanol-hexane solvent system. In case of all the cocrystals, it is observed that the fluorescence intensity of the mixture gradually increases with the increase in percentage of hexane but not to a significant extent (Figure S27-35).

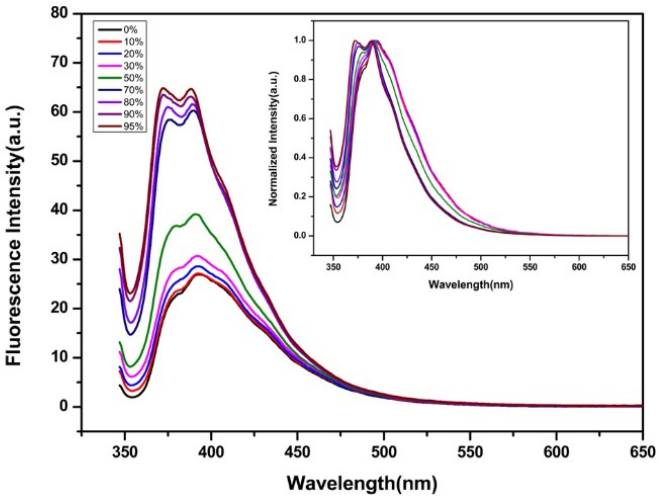

(a)

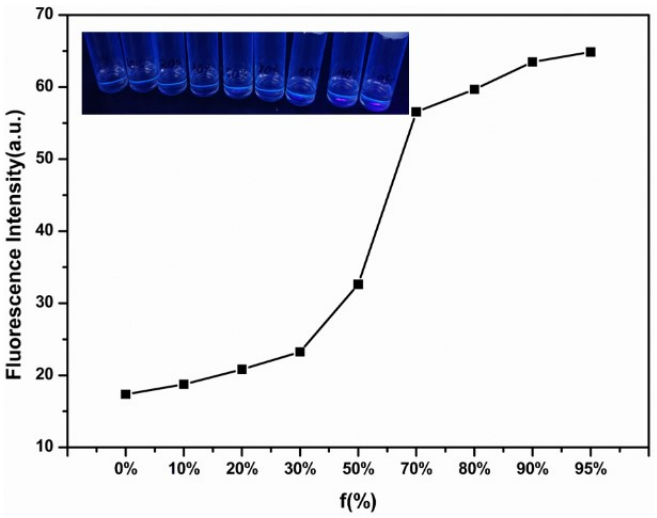

(b)

Figure S28. Fluorescence spectra of the **PDAN-1•OA** in ethanol–hexane with different hexane percentage (%) at an exciting wavelength 337 nm (b) Plot of fluorescence intensity at 372.06 nm with the varying percentage of hexane (%).

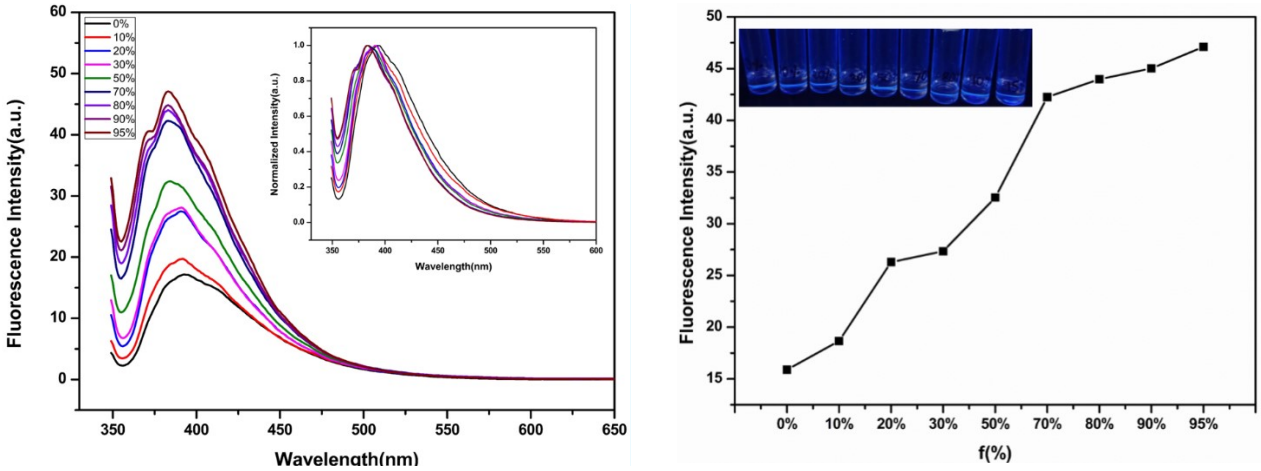

(a) (b)

Figure S29. (a) Fluorescence spectra of the **PDAN-1•MA** in ethanol–hexane with different hexane percentage (%) at an exciting wavelength 339 nm (b) Plot of fluorescence intensity at 382.96 nm with the varying percentage of hexane (%).

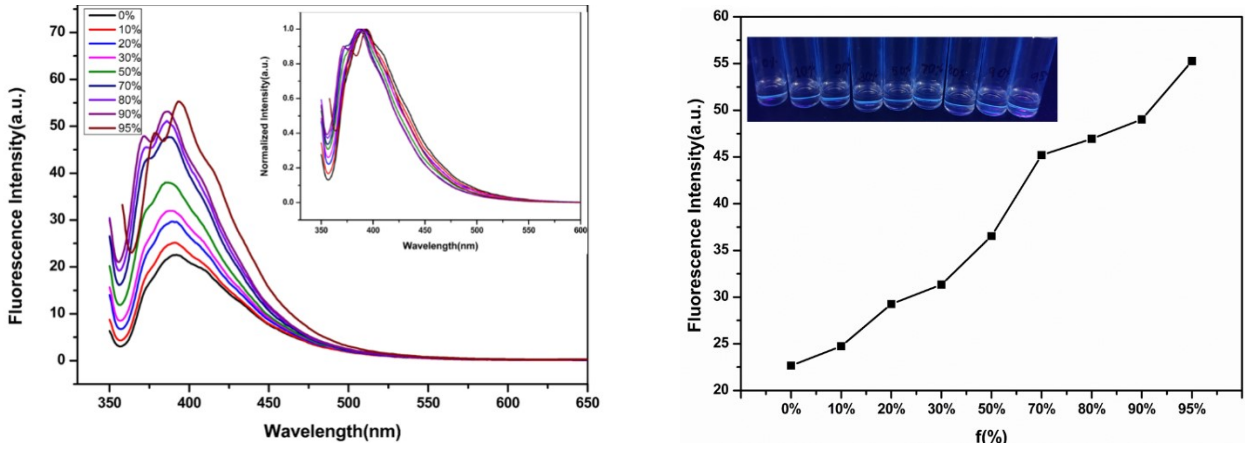

(a) (b)

Figure S30. (a) Fluorescence spectra of the **PDAN-1•SA** in ethanol–hexane with different hexane percentage (%) at an exciting wavelength 340 nm (b) Plot of fluorescence intensity at 393.59 nm with the varying percentage of hexane (%).

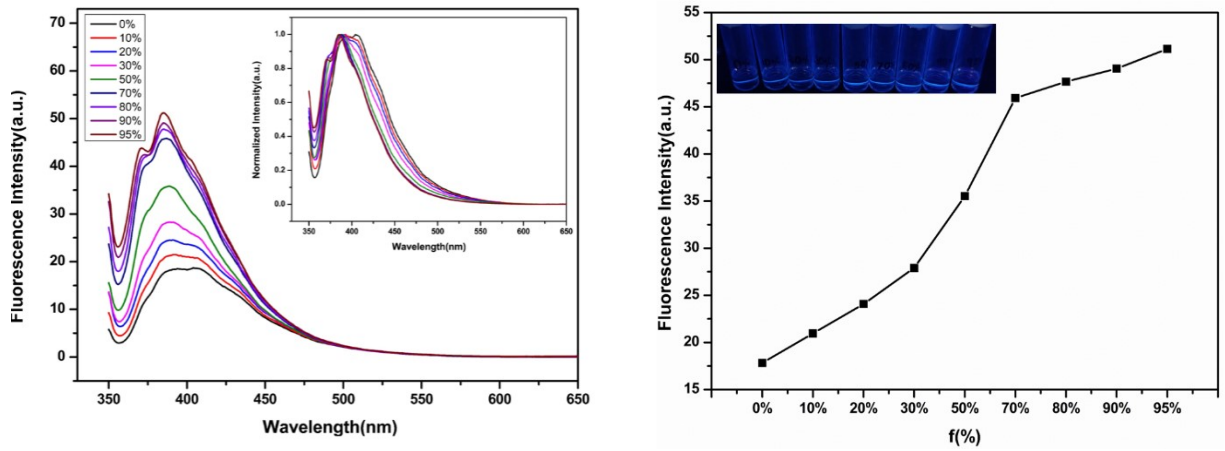

(a) (b)

Figure S31. (a) Fluorescence spectra of the **PDAN-1•GA** in ethanol–hexane with different hexane percentage (%) at an exciting wavelength 340 nm (b) Plot of fluorescence intensity at 385.17 nm with the varying percentage of hexane (%).

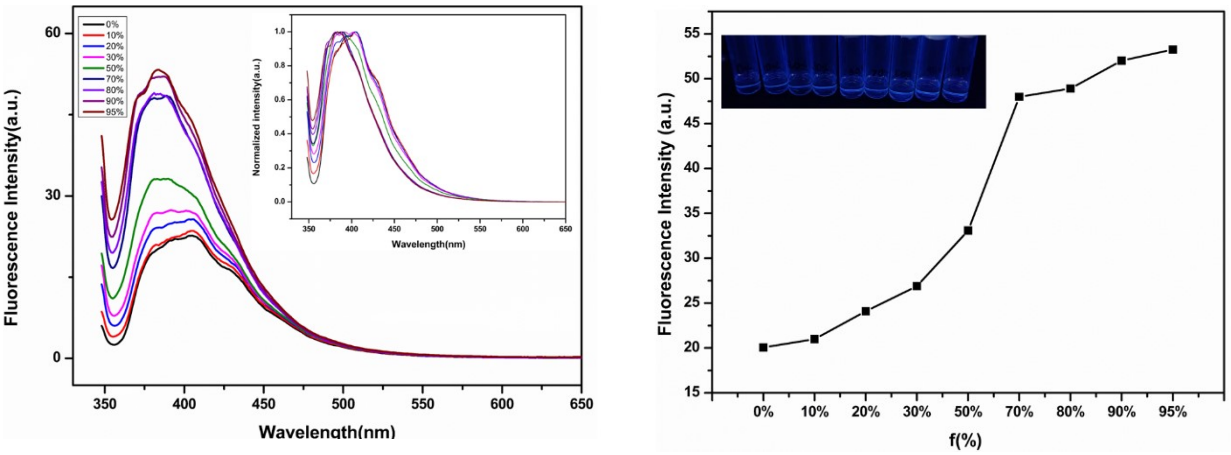

(a) (b)

Figure S32. (a) Fluorescence spectra of the **PDAN-1•AA** in ethanol–hexane with different hexane percentage (%) at an exciting wavelength 337 nm (b) Plot of fluorescence intensity at 383.76 nm with the varying percentage of hexane (%).

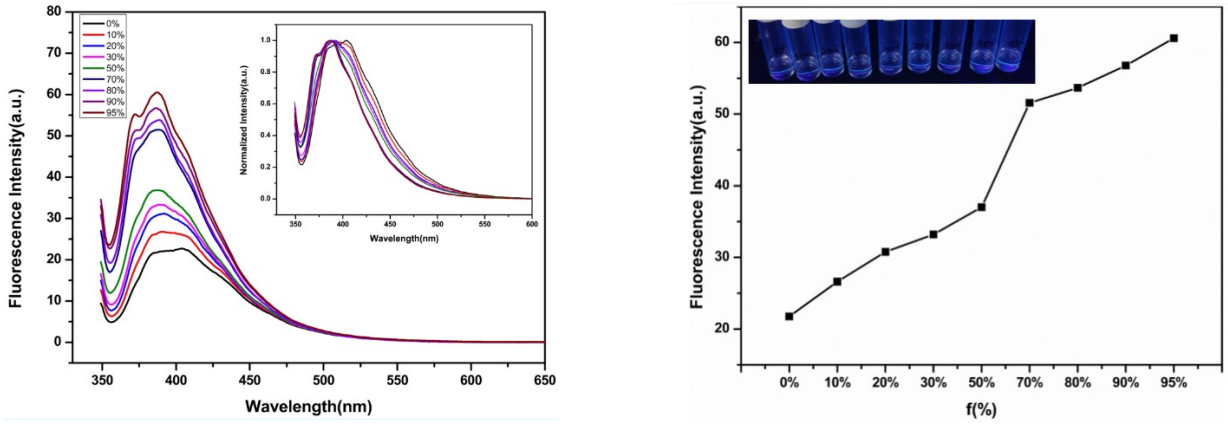

(a) (b)

Figure S33. (a) Fluorescence spectra of the **PDAN-1•PA** in ethanol–hexane with different hexane percentage (%) at an exciting wavelength 339 nm (b) Plot of fluorescence intensity at 387.11 nm with the varying percentage of hexane (%).

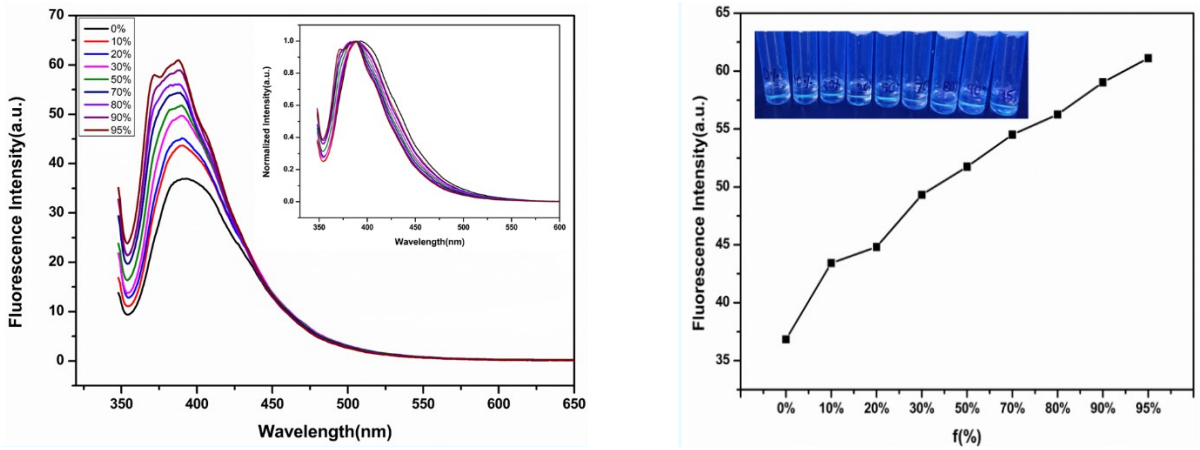

(a) (b)

Figure S34. (a) Fluorescence spectra of the **PDAN-1•SUBE** in ethanol–hexane with different hexane percentage (%) at an exciting wavelength 338 nm (b) Plot of fluorescence intensity at 387.91 nm with the varying percentage of hexane (%).

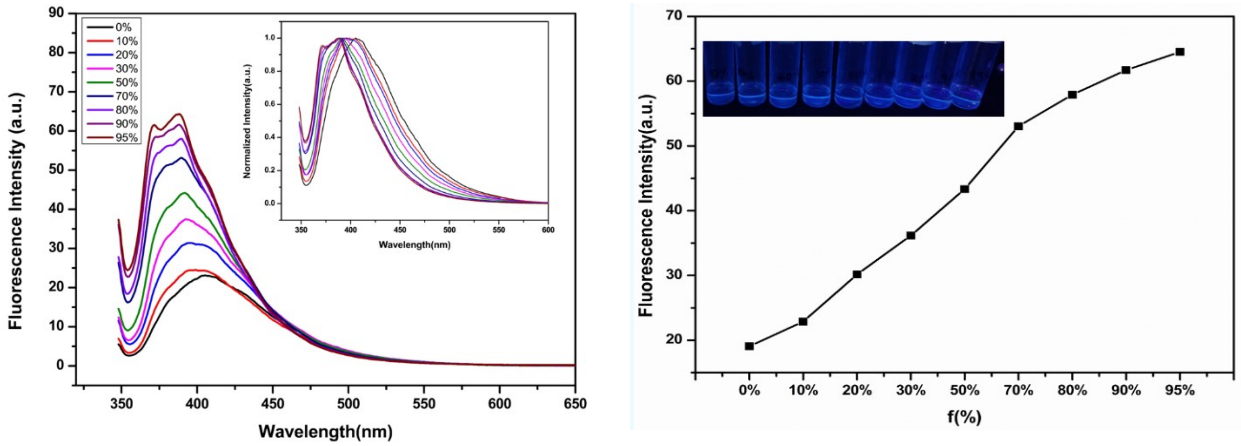

(a) (b)

Figure S35. (a) Fluorescence spectra of the **PDAN-1•AZA** in ethanol–hexane with different hexane percentage (%) at an exciting wavelength 338 nm (b) Plot of fluorescence intensity at 388.20 nm with the varying percentage of hexane (%).

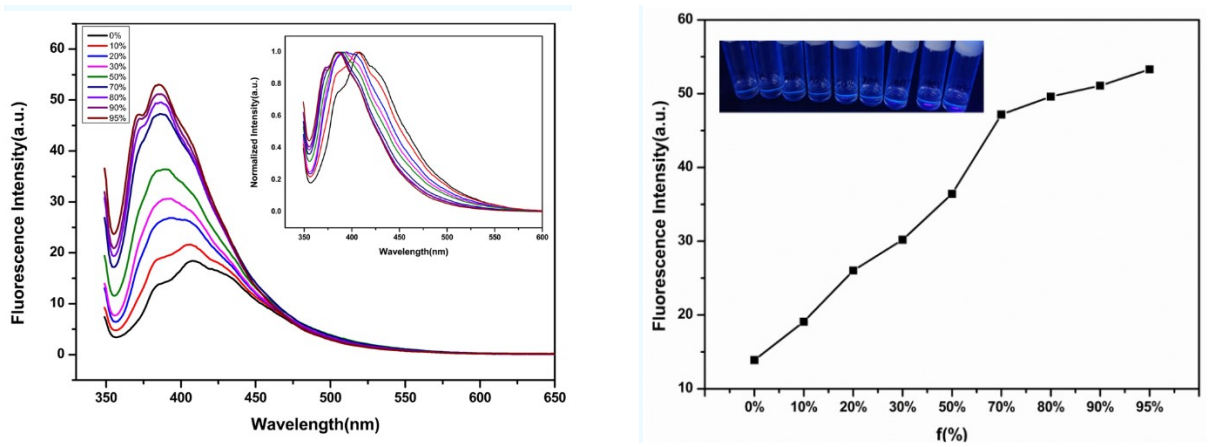

(a) (b)

Figure S36. (a) Fluorescence spectra of the **PDAN-1•SEBA** in ethanol–hexane with different hexane percentage (%) at an exciting wavelength 339 nm (b) Plot of fluorescence intensity at 385.30 nm with the varying percentage of hexane (%).

11. DSC thermograms of PDAN-1 multicomponent solids

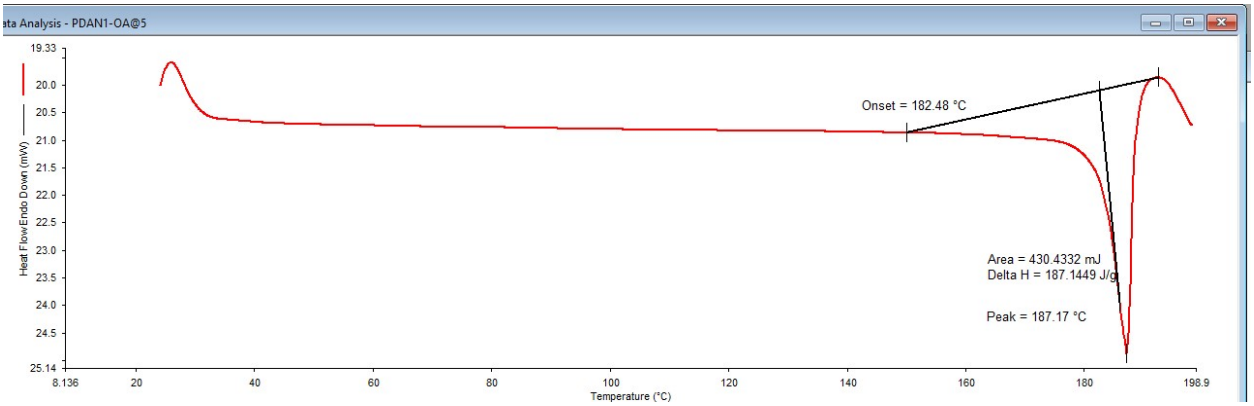

(a)

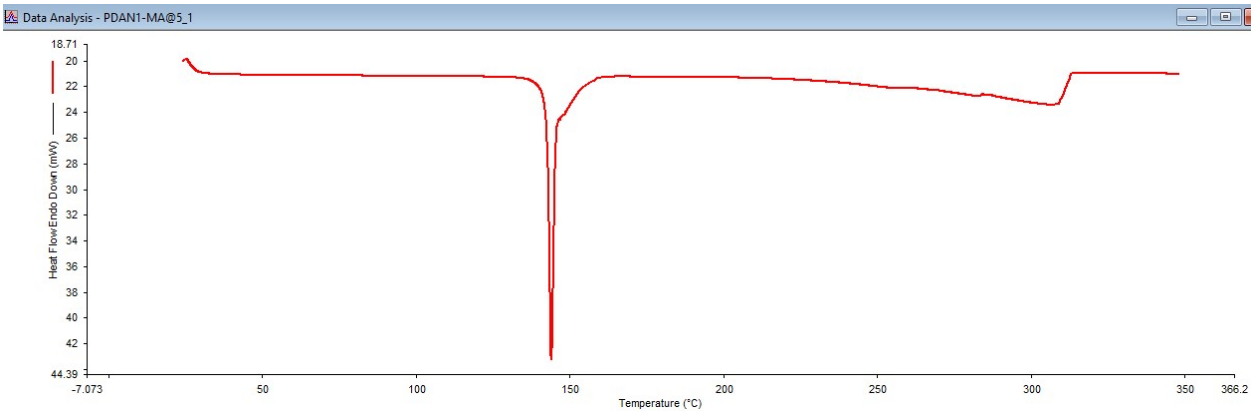

(b)

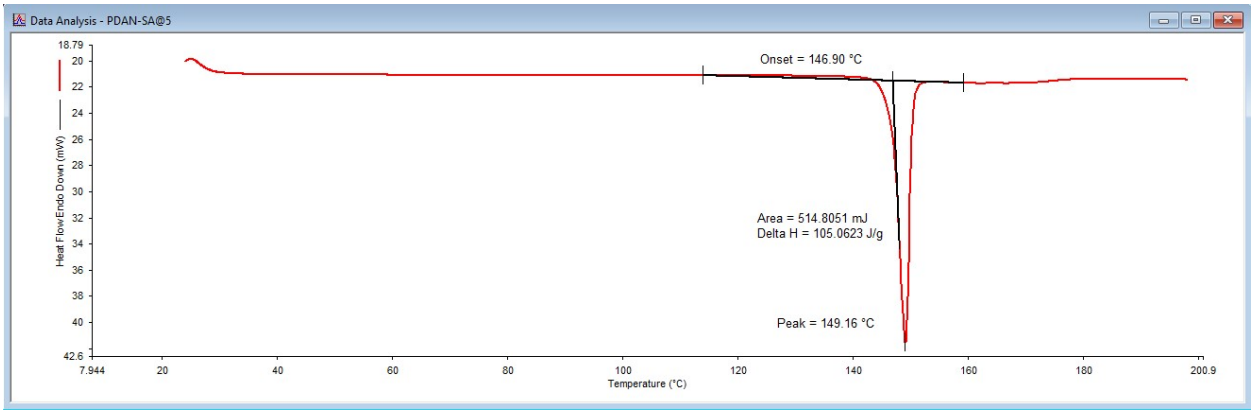
Data Analysis - PDAN-SA@5
Heat Flow Endo Down (mW)
Temperature (°C)
Onset = 146.90 °C
Area = 514.8051 mJ
Delta H = 105.0623 J/g
Peak = 149.16 °C

(c)

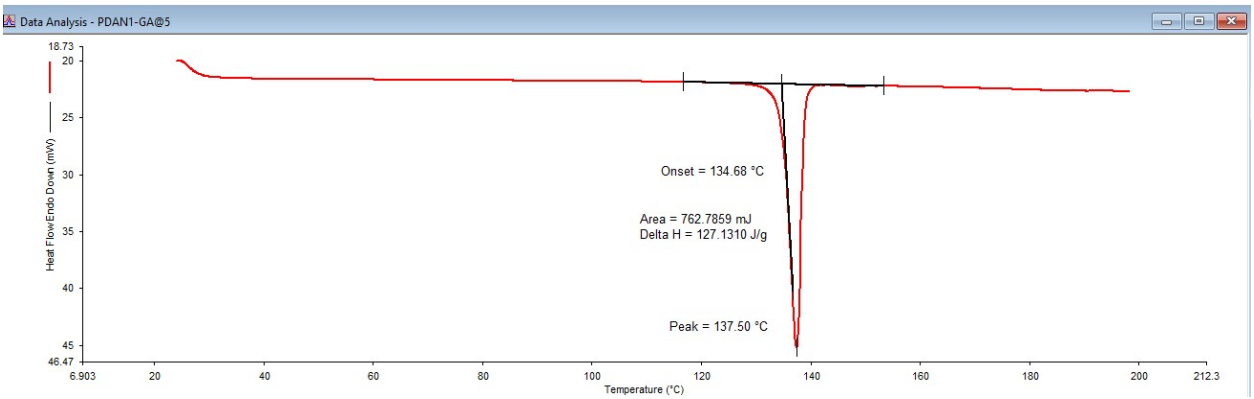
Data Analysis - PDAN1-GA@5
Heat Flow Endo Down (mW)
Temperature (°C)
Onset = 134.68 °C
Area = 762.7859 mJ
Delta H = 127.1310 J/g
Peak = 137.50 °C

(d)

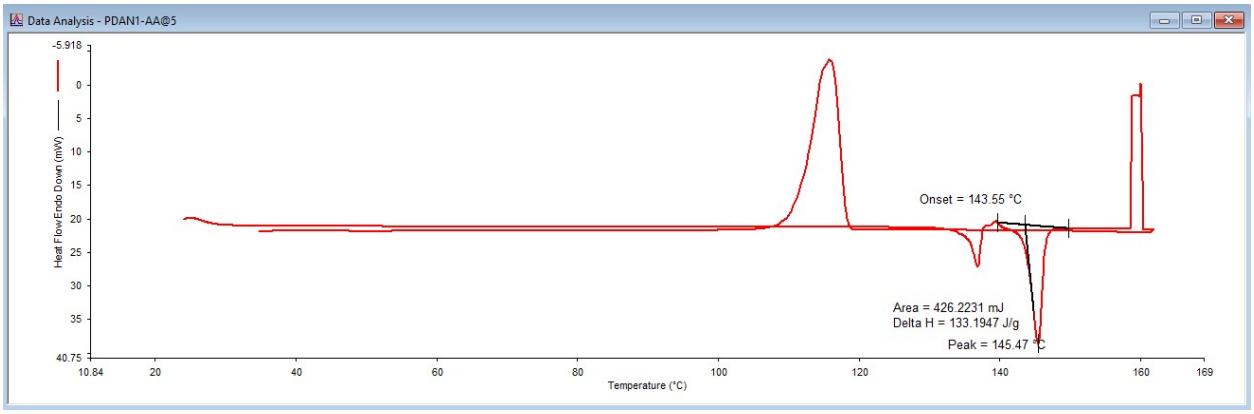
Data Analysis - PDAN1-AA@5
Heat Flow Endo Down (mW)
Temperature (°C)
Onset = 143.55 °C
Area = 426.2231 mJ
Delta H = 133.1947 J/g
Peak = 145.47 °C

(e)

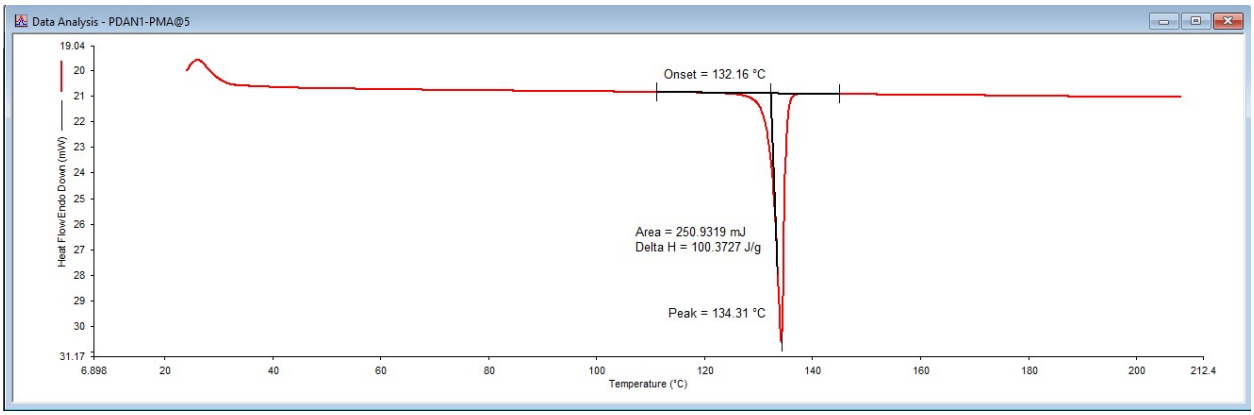
Data Analysis - PDAN1-PMA@5
Onset = 132.16 °C
Area = 250.9319 mJ
Delta H = 100.3727 J/g
Peak = 134.31 °C
Heat Flow Endo Down (mW)
Temperature (°C)

(f)

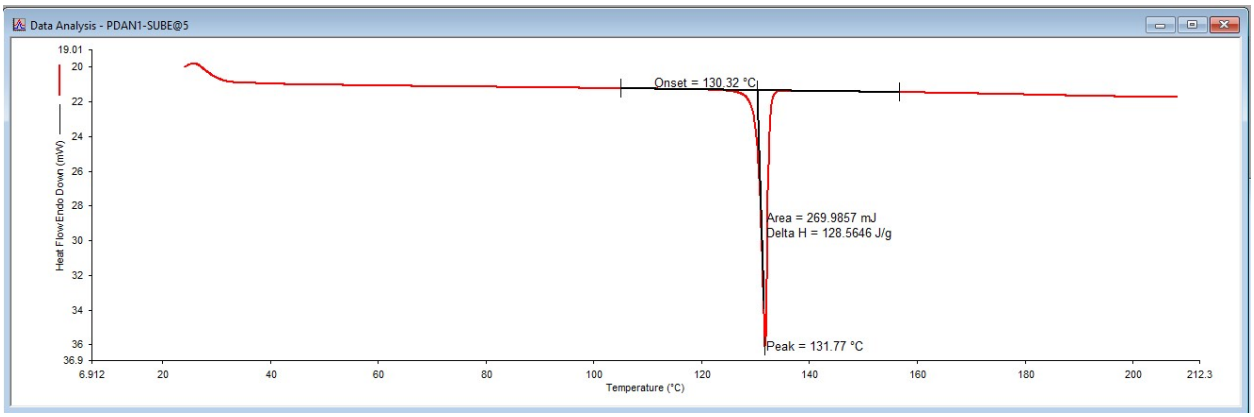
Data Analysis - PDAN1-SUBE@5
Onset = 130.32 °C
Area = 269.9857 mJ
Delta H = 128.5646 J/g
Peak = 131.77 °C
Heat Flow Endo Down (mW)
Temperature (°C)

(g)

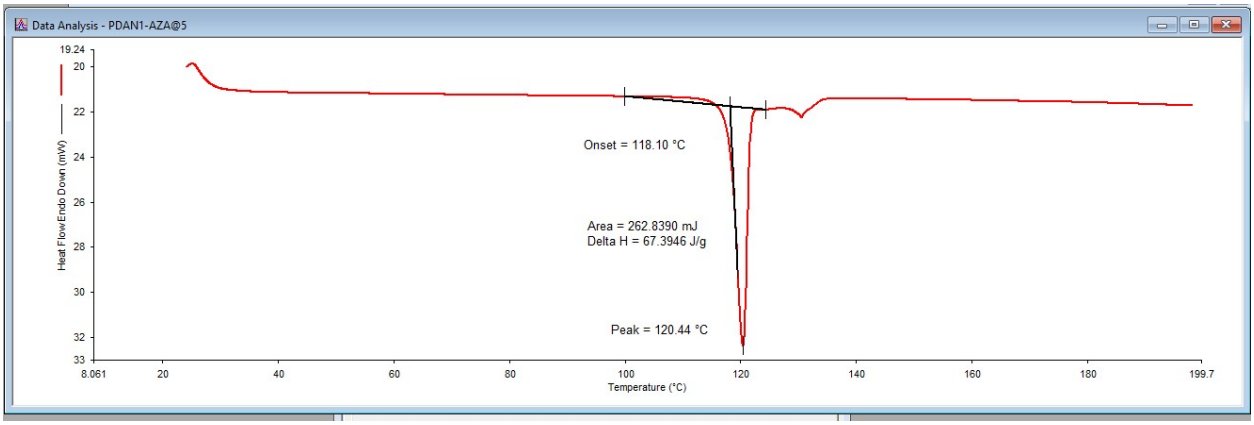
Data Analysis - PDAN1-AZA@5
Onset = 118.10 °C
Area = 262.8390 mJ
Delta H = 67.3946 J/g
Peak = 120.44 °C
Heat Flow Endo Down (mW)
Temperature (°C)

(h)

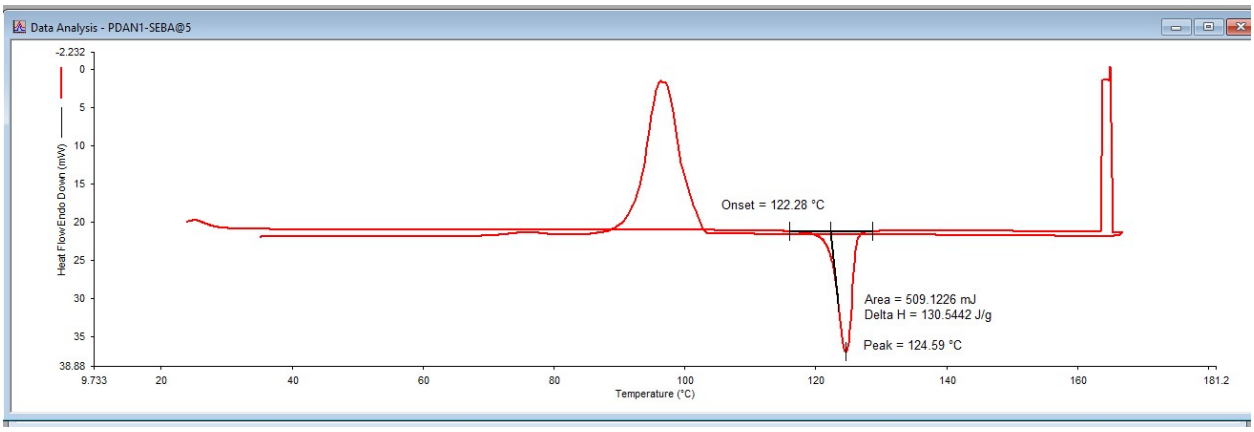

(i)

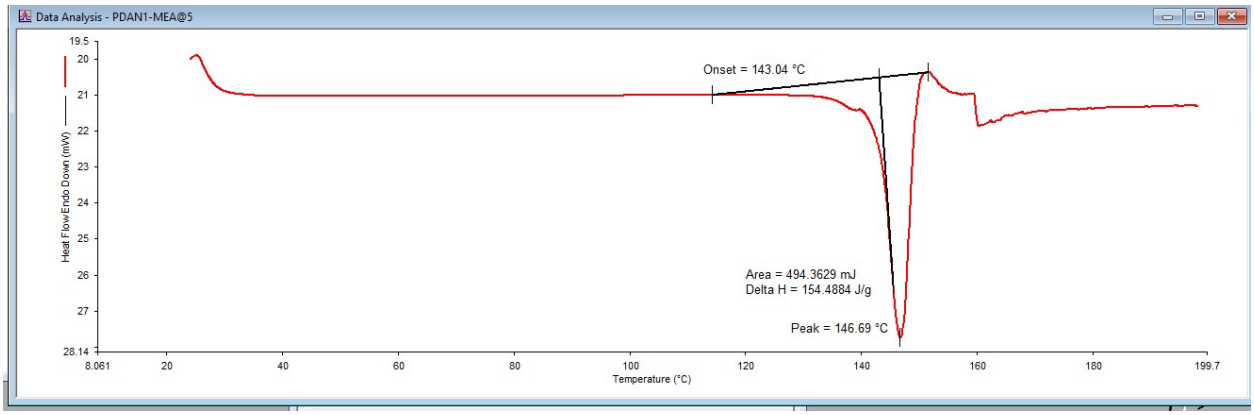

(j)

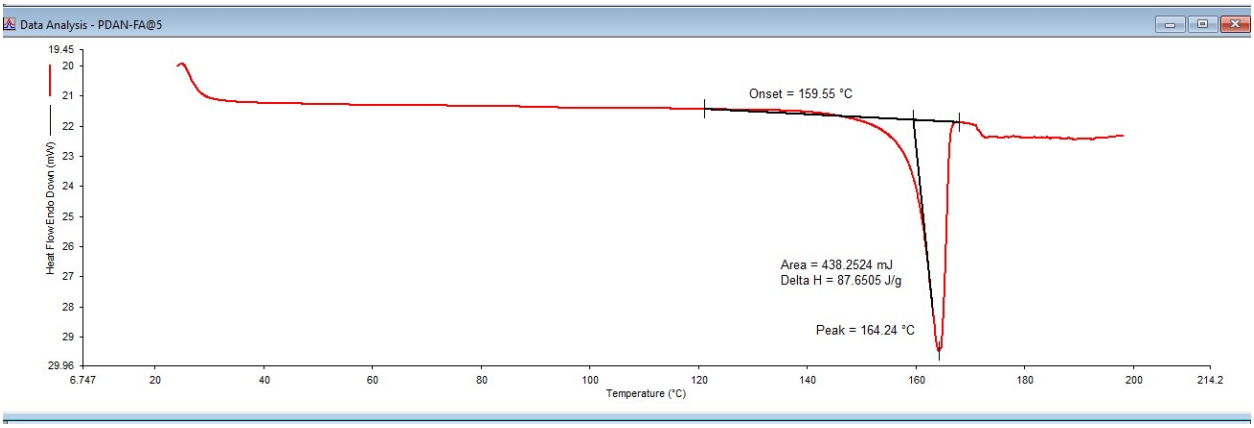

(k)

Figure S37. DSC thermogram of **PDAN-1P** multi-component solids with coformers (a) OA, (b) MA, (c) SA, (d) GA, (e) AA, (f) PMA, (g) SUBE, (h) AZA, (i) SEBA, (j) MEA and (k) FA.

12. Nanomechanical analysis

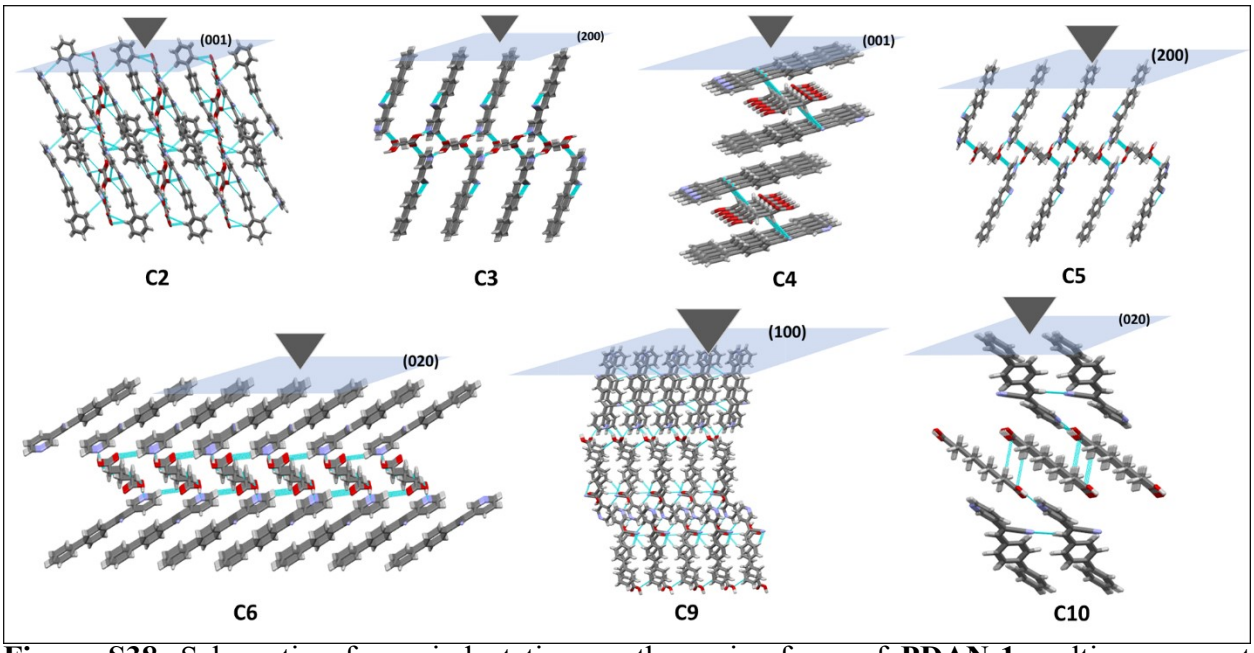

Figure S38. Schematic of nanoindentation on the major faces of **PDAN-1** multi-component solids with all the aliphatic dicarboxylic acid coformers used in the study derived from BFDH morphology.

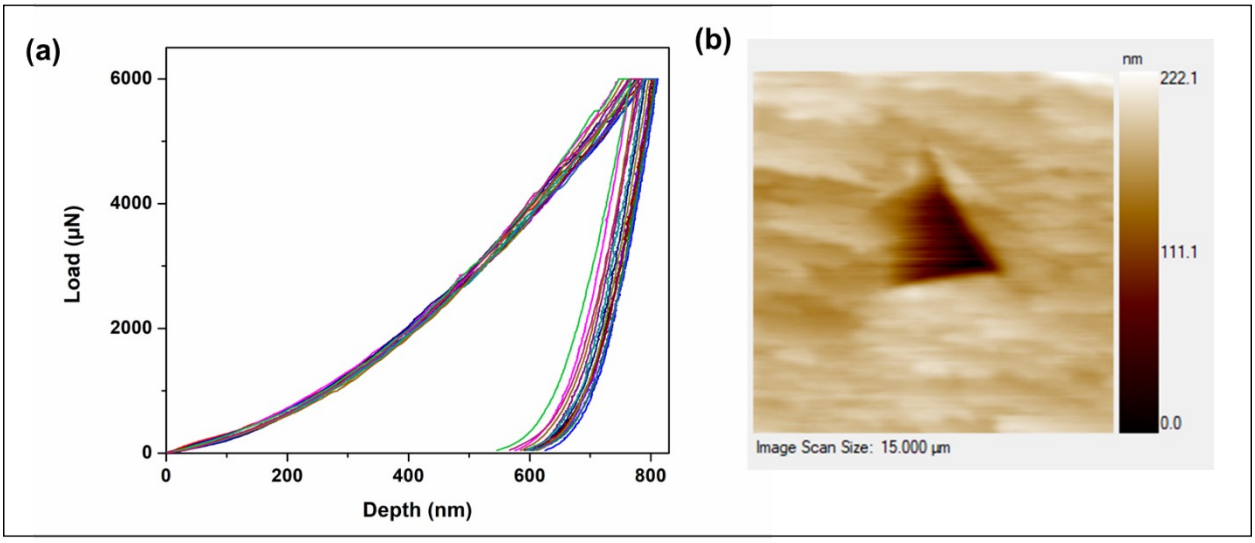

Figure S39. (a) Representative load-depth (*P*–*h*) curves obtained using peak load of 6 mN on major face of **PDAN-1•OA** salt cocrystal. (b) 2D representation of the scanning probe microscopic (SPM) image of the residual indent impression. The reduced modulus obtained is 15.32±1.02 GPa.

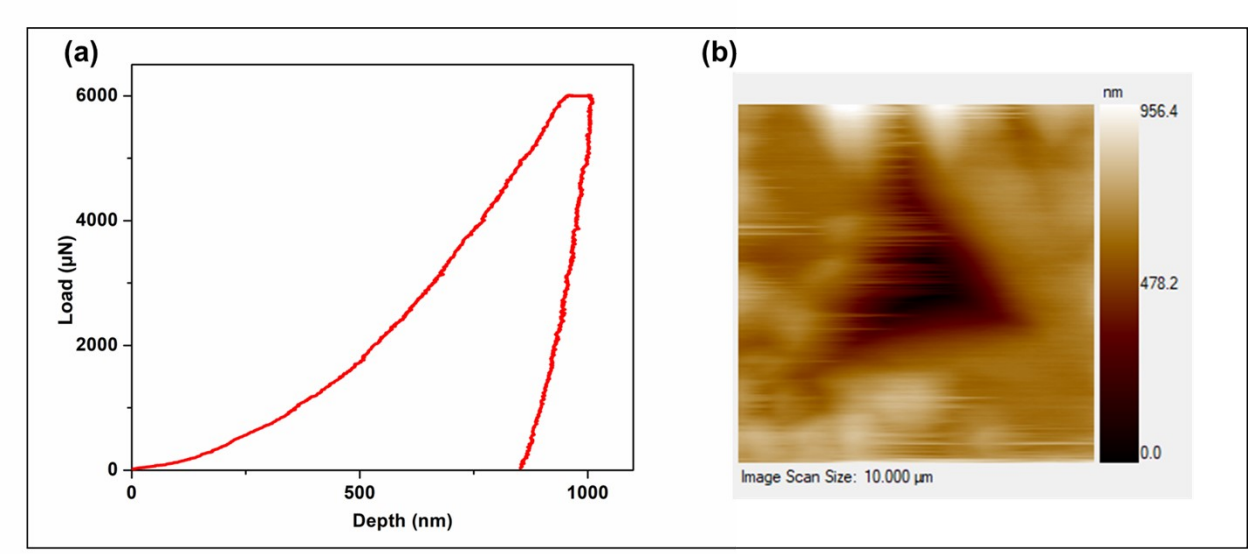

Figure S40. (a) Representative load-depth (*P*–*h*) curves obtained using peak load of 6 mN on major face of **PDAN-1•MA** cocrystal. (b) 2D representation of the scanning probe microscopic (SPM) image of the residual indent impression. The reduced modulus obtained is 11.78±2.97 GPa.

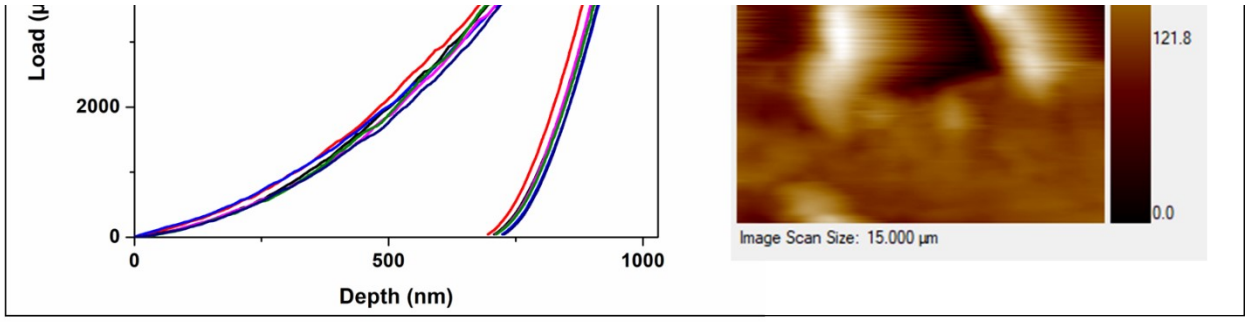

Figure S41. (a) Representative load-depth (*P*–*h*) curves obtained using peak load of 6 mN on major face of **PDAN-1•SA** cocrystal. (b) 2D representation of the scanning probe microscopic (SPM) image of the residual indent impression. The reduced modulus obtained is 7.82±0.17 GPa.

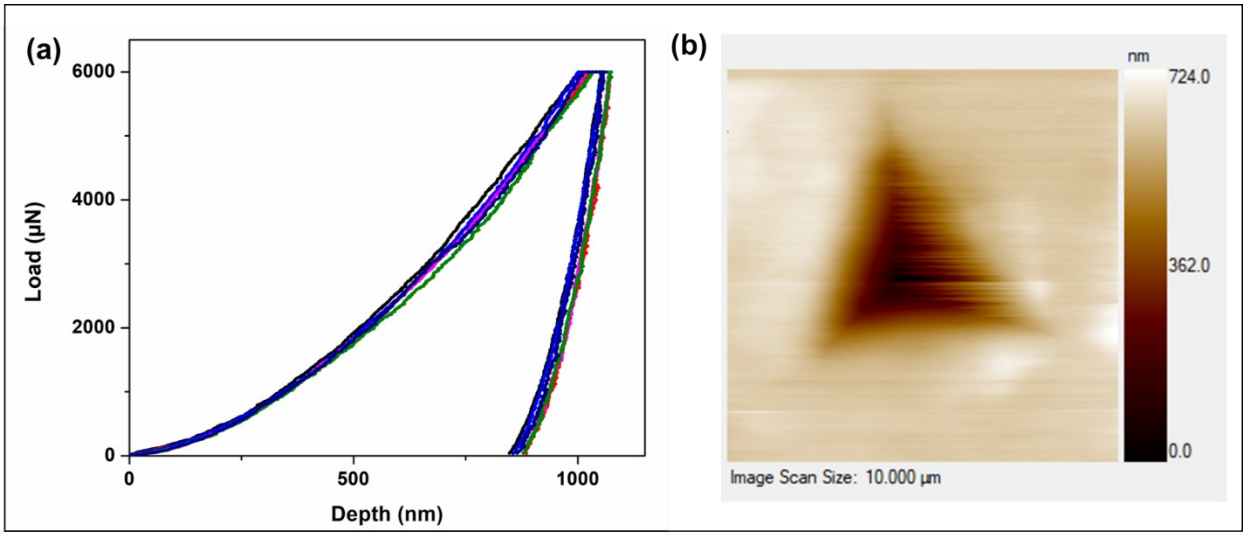

Figure S42. (a) Representative load-depth (P–h) curves obtained using peak load of 6 mN on major face of **PDAN-1•GA** cocrystal. (b) 2D representation of the scanning probe microscopic (SPM) image of the residual indent impression. The reduced modulus obtained is 9.13±0.24 GPa.

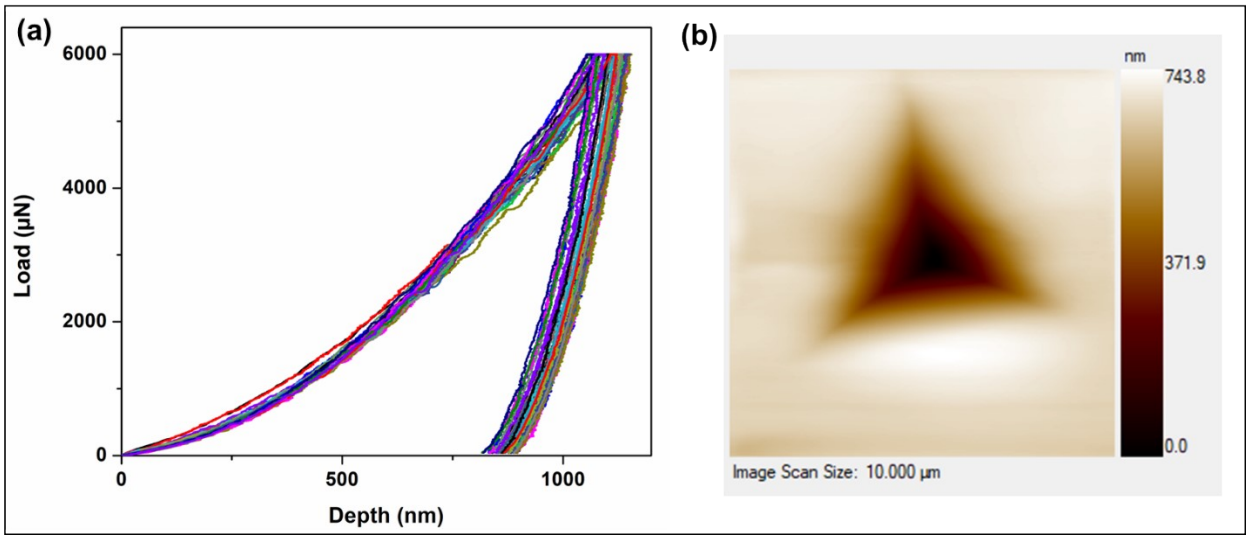

Figure S43. (a) Representative load-depth (*P–h*) curves obtained using peak load of 6 mN on major face of **PDAN-1•AA** cocrystal. (b) 2D representation of the scanning probe microscopic (SPM) image of the residual indent impression. The reduced modulus obtained is 6.86±0.55 GPa.

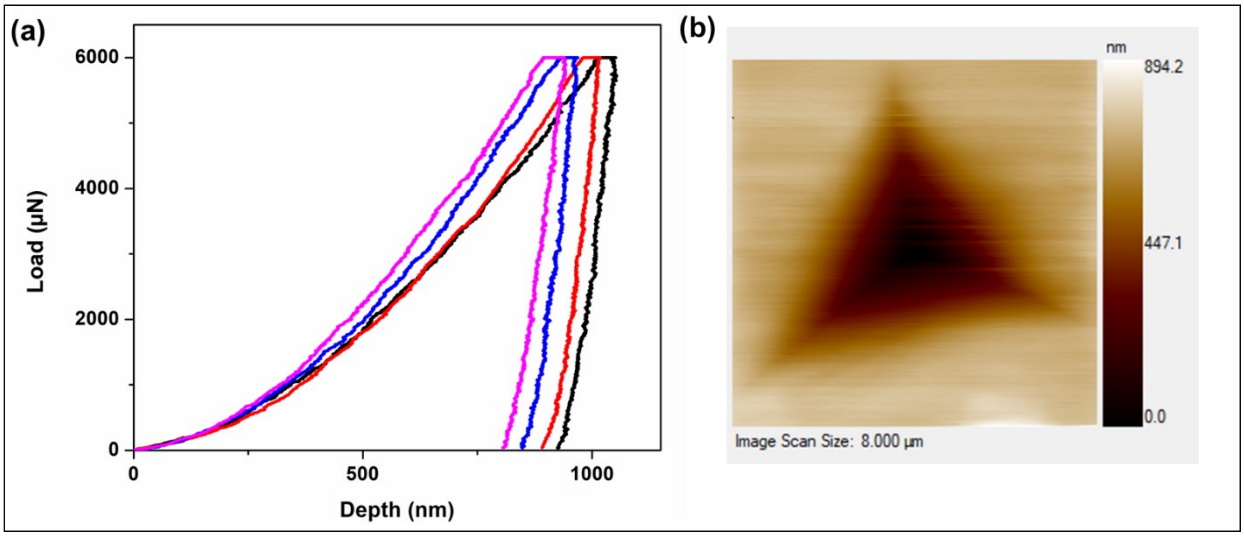

Figure S44. (a) Representative load-depth (P–h) curves obtained using peak load of 6 mN on major face of **PDAN-1•AZA** cocrystal. (b) 2D representation of the scanning probe microscopic (SPM) image of the residual indent impression. The reduced modulus obtained is 13.07±1.20 GPa.

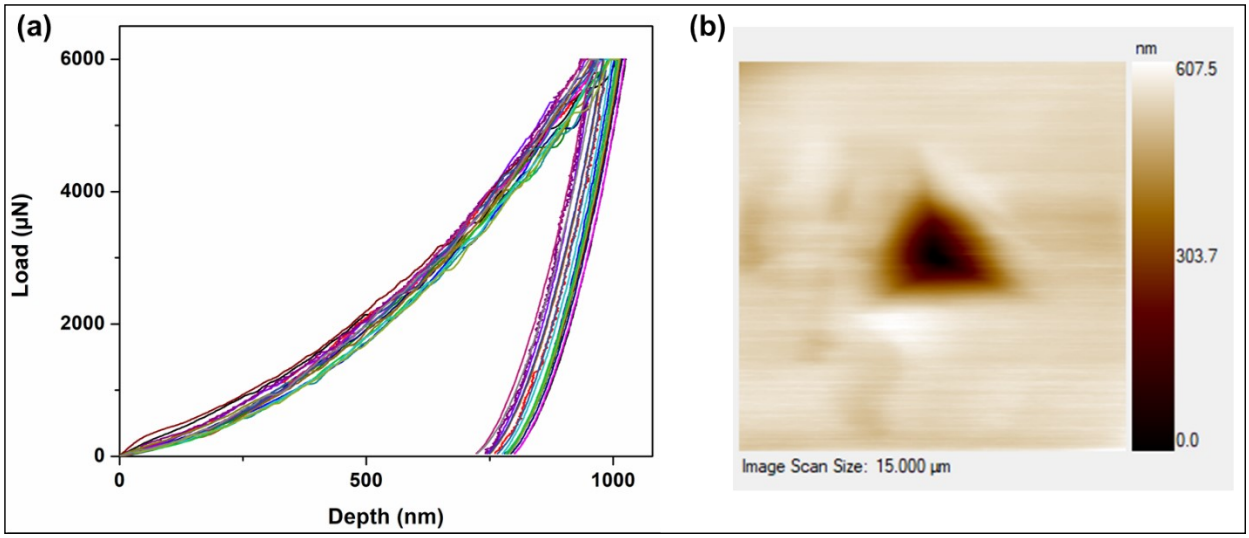

Figure S45. (a) Representative load-depth (*P*–*h*) curves obtained using peak load of 6 mN on major face of **PDAN-1•SEBA** cocrystal. (b) 2D representation of the scanning probe microscopic (SPM) image of the residual indent impression. The reduced modulus obtained is 8.59±0.34 GPa.